

Altered Hippocampal Place Cell Representation and Theta Rhythmicity following Moderate Prenatal Alcohol Exposure

Highlights

- Prenatal alcohol exposure reduces place field spatial tuning and stability
- Prenatal alcohol exposure decreases place field directionality on the linear track
- Prenatal alcohol exposure increases control of place fields by a proximal cue
- Prenatal alcohol exposure slows theta oscillations and alters phase precession

Authors

Ryan E. Harvey, Laura E. Berkowitz,
Daniel D. Savage, Derek A. Hamilton,
Benjamin J. Clark

Correspondence

bnjclark@unm.edu

In Brief

Harvey et al. demonstrate that prenatal alcohol exposure disrupts hippocampal place cell firing and slows theta oscillations. The findings represent a critical step in developing a complete multi-level understanding of the neurobiological basis of spatial learning and memory impairments after moderate prenatal alcohol exposure.

Article

Altered Hippocampal Place Cell Representation and Theta Rhythmicity following Moderate Prenatal Alcohol Exposure

Ryan E. Harvey,¹ Laura E. Berkowitz,¹ Daniel D. Savage,^{1,2} Derek A. Hamilton,^{1,2} and Benjamin J. Clark^{1,2,3,*}

¹Department of Psychology, University of New Mexico, 2001 Redondo S Drive, Albuquerque, NM 87106, USA

²Department of Neurosciences, University of New Mexico, 900 Camino de Salud, Albuquerque, NM 87131, USA

³Lead Contact

*Correspondence: bnjclark@unm.edu

<https://doi.org/10.1016/j.cub.2020.06.077>

SUMMARY

Prenatal alcohol exposure (PAE) leads to profound deficits in spatial memory and synaptic and cellular alterations to the hippocampus that last into adulthood. Neurons in the hippocampus called place cells discharge as an animal enters specific places in an environment, establish distinct ensemble codes for familiar and novel places, and are modulated by local theta rhythms. Spatial memory is thought to critically depend on the integrity of hippocampal place cell firing. Therefore, we tested the hypothesis that hippocampal place cell firing is impaired after PAE by performing *in vivo* recordings from the hippocampi (CA1 and CA3) of moderate PAE and control adult rats. Our results show that hippocampal CA3 neurons from PAE rats have reduced spatial tuning. Second, CA1 and CA3 neurons from PAE rats are less likely to orthogonalize their firing between directions of travel on a linear track and between changes in contextual stimuli in an open arena compared to control neurons. Lastly, reductions in the number of hippocampal place cells exhibiting significant theta rhythmicity and phase precession were observed, which may suggest changes to hippocampal microcircuit function. Together, the reduced spatial tuning and sensitivity to contextual changes provide a neural systems-level mechanism to explain spatial memory impairment after moderate PAE.

INTRODUCTION

Prenatal alcohol exposure (PAE) is detrimental to the developing nervous system [1] and remains one of the most common developmental insults [2–4]. Globally, 9.8% of individuals consume alcohol while pregnant [5]. There is a large body of evidence supporting the conclusion that even a moderate amount of alcohol exposure during fetal development (blood alcohol concentration [BAC] 7–120 mg/dL) can disrupt the synaptic and cellular networks believed to underlie episodic and spatial memory, resulting in significant lifelong deficits in the ability to remember locations and effectively navigate [6–10].

The hippocampus is critical for the encoding of spatial [11] and episodic memories [12, 13]. The hippocampal (HPC) subregions dentate gyrus, CA1, CA2, and CA3 contain neurons called “place cells” that selectively fire at particular positions of an animal’s path, resulting in receptive fields for particular locations in space [14, 15]. These receptive fields are referred to as place fields, and their precise population activity has been thought to form a “cognitive map,” giving an animal a sense of past, present, and future locations [16]. Although the correlation between a place cell’s firing rate and location is commonly referred to as rate coding, phase or temporal coding co-occurs, whereby spikes from single theta-rhythmic place cells systematically phase shift across successive theta cycles in a phenomenon known as theta phase precession [17].

Moderate PAE during the first and second trimester impairs spatial behavior (reviewed in [7]). In the Morris water task, rats with moderate PAE are generally unable to quickly adapt to changes in task demands, such as a change in the escape location in the water task or recalling a previously learned location [9, 18–20]. In dry land tasks, moderate PAE impairs spatial discrimination [21, 22], with greater deficits observed when the discrimination involves subtle differences in spatial context [21]. Importantly, spatial flexibility and discrimination are thought to be reliant on functionally intact hippocampi and have been associated with HPC place cell activity [23, 24].

Moderate PAE can also lead to reductions in long-term potentiation (LTP), which is considered to be a mechanism by which increases in synaptic strength support associative learning [25, 26]. The most prominent reductions in LTP are observed in the dentate gyrus following perforant path stimulation [27–29] and may be related to alterations in N-methyl-D-aspartate (NMDA) subunit composition [27]. Importantly, reductions in LTP or NMDA receptor function have been linked to a loss in the spatial stability of HPC place fields [30–36] and their failure to remap or discriminate spatial contexts [37] (discussed in [38]). Thus, it is expected that HPC-dependent spatial discrimination, such as how place cells discriminate directions of locomotion on linear track environments [39–41] or between spatial context changes [38], will be disrupted following PAE.

The linkage between spatial behavior and HPC structural differences after moderate PAE is poorly understood but is likely to involve alterations in HPC place cell activity [7]. Although previous studies have shown acute alcohol exposure in adult rats disrupts HPC place cell activity [42, 43], we are unaware of prior work investigating the impact of developmental alcohol exposure on HPC place cell activity. Thus, in the present study, we first hypothesized that, because PAE impairs spatial behavior and HPC function, place cells will have altered spatial tuning, temporal-spatial stability, theta rhythmicity, and phase coding in PAE offspring. Second, because previous studies report decreased LTP, we hypothesize that place cells from rats with PAE will have decreased directional discrimination on a linear track environment and differential rate and spatial tuning effects following contextual stimuli changes between sessions. Therefore, we recorded from neurons from HPC CA1 and CA3 of adult rats with moderate PAE (BAC: 60.8 ± 5.8 mg/dL) [44] that occurred throughout gestation, and saccharin control rats over three environmental conditions: a linear track; an open field cylinder; and an open field cylinder with a proximal cue rotation (Figures 1A and 1B). Although firing responses to spatial features have been observed to differ between CA1 and CA3 subregions [45–49], the following analyses focus on assessing intraregional comparisons between PAE and control cell populations. Our results show that HPC CA3 neurons from PAE rats have reduced spatial tuning and are less likely to display theta phase precession. Second, CA1 and CA3 neurons from PAE rats have reduced theta frequencies and are less likely to orthogonalize their firing between directions of travel on the linear track and in contextual stimuli changes between the cylinder sessions compared to control animals.

RESULTS

Reduction in Spatial Tuning of CA3 Place Cells after PAE

To explore how HPC spatial encoding is affected following moderate PAE, we recorded populations of HPC neurons from 9 control and 8 PAE adult male rats as they ran laps on a linear track or randomly foraged for scattered food in a cylindrical enclosure (Figures 1A and 1B). PAE did not disrupt the ability to perform laps on the linear track, with no group differences observed in the number of laps completed per session (control median: 41; PAE median: 40). Similarly, there were no significant group differences in trial-averaged running speed on the linear track or in the cylinder (discussed in section *Speed-Modulated Intrinsic Theta Frequency*). These findings are consistent with previous studies that have reported unaffected locomotor behaviors following moderate PAE [21, 50].

Despite similar behavioral metrics, impairments in the spatial tuning, measured by spatial information content and sparsity, were evident in PAE place fields. CA3 place fields in PAE animals had significantly lower spatial information and higher sparsity in both linear track and cylinder tests ($p < 0.001$; Wilcoxon rank-sum [WRS]; effect sizes [r] ≥ 0.19 ; Figure 1C). In contrast, we did not observe group differences in spatial tuning by CA1 place fields.

We also investigated group differences in peak firing rate and spatial coherence, which measures the consistency of spiking across the place field. In PAE rats, CA1 and CA3 place cells had significantly diminished peak firing rates in both tasks ($p <$

0.05; WRS; effect sizes [r] ≥ 0.10 ; Figure 1C). Average firing rates and bursting across sessions are shown in Figure S1. Furthermore, CA1 and CA3 firing fields in PAE rats had significantly lower spatial coherence in both tasks ($p < 0.05$; WRS; effect sizes [r] ≥ 0.08 ; Figure 1C). However, it is important to note that the extent of these two CA1 differences were small (effect sizes [r] 0.10–0.14). Together, these results indicate that peak firing and coherence in both CA1 and CA3 were affected by PAE and measures of spatial tuning were affected in CA3.

Reduced within-Session Stability by CA1 and CA3 Place Cells after PAE

To investigate whether spatial tuning was stable over time, we evaluated the within-session spatial stability of place fields on the linear track and cylinder environments (Figure 2). Within-session stability was measured by calculating the spatial correlation between rate maps generated from the first half of the recording session versus the second half. CA1 and CA3 PAE place cells had lower within-session stability compared to control CA1 and CA3 place cells in both linear track and cylinder environments ($p < 0.001$; WRS; effect sizes [r] ≥ 0.11 ; Figure 2). To ensure that these results were not due to poor sampling of the environment, we assessed running speed and the amount of exploration across the two halves of each recording session (Figure S2). Although running speeds and amount of exploration was similar between groups in the cylinder, running speeds from PAE rats on the linear track tended to slightly increase (1 cm/s) from the first to second half of each session compared to control rats. However, because place cell firing properties tend to scale with running speed [51, 52], indicating that stable representations are possible during fast and slow running epochs, and both groups had a similar amount of exploration between the two halves, the difference in speed is unlikely to have negatively affected stability. Together, the decreased spatial stability suggests that PAE negatively affects the ability to create stable spatial representations over relatively short timescales.

Reduced CA1 and CA3 Place Cell Directionality after PAE

When rodents engage in random foraging in an open-field environment, place cells exhibit location-specific firing that is often independent of the direction of travel through the place field [53]. However, when the animal's path is restricted, such as in a linear track, firing rates and peak firing locations significantly differ in opposite directions of travel [39, 41, 54]. As a result, place cells express directionality in their firing such that their representation of the track in the two directions are distinct or orthogonal (Figures 3A and 3B). Thus, to determine whether directional firing on the linear track was impaired after PAE, we quantified place cell directionality in two ways: first by correlating rate maps for place fields in each direction of travel and by computing a directionality index that quantifies the magnitude of firing rate differences between each direction of travel. We found that spatial correlations between the two running directions were significantly higher for CA1 PAE place cells ($p < 0.01$; WRS; effect size [r] = 0.17; Figures 3A–3C) but were similar across the two groups for CA3 place cells ($p > 0.05$; WRS). Indicating that, following PAE, CA1 place cells on the linear track are less likely to spatially orthogonalize. Similarly, the directionality

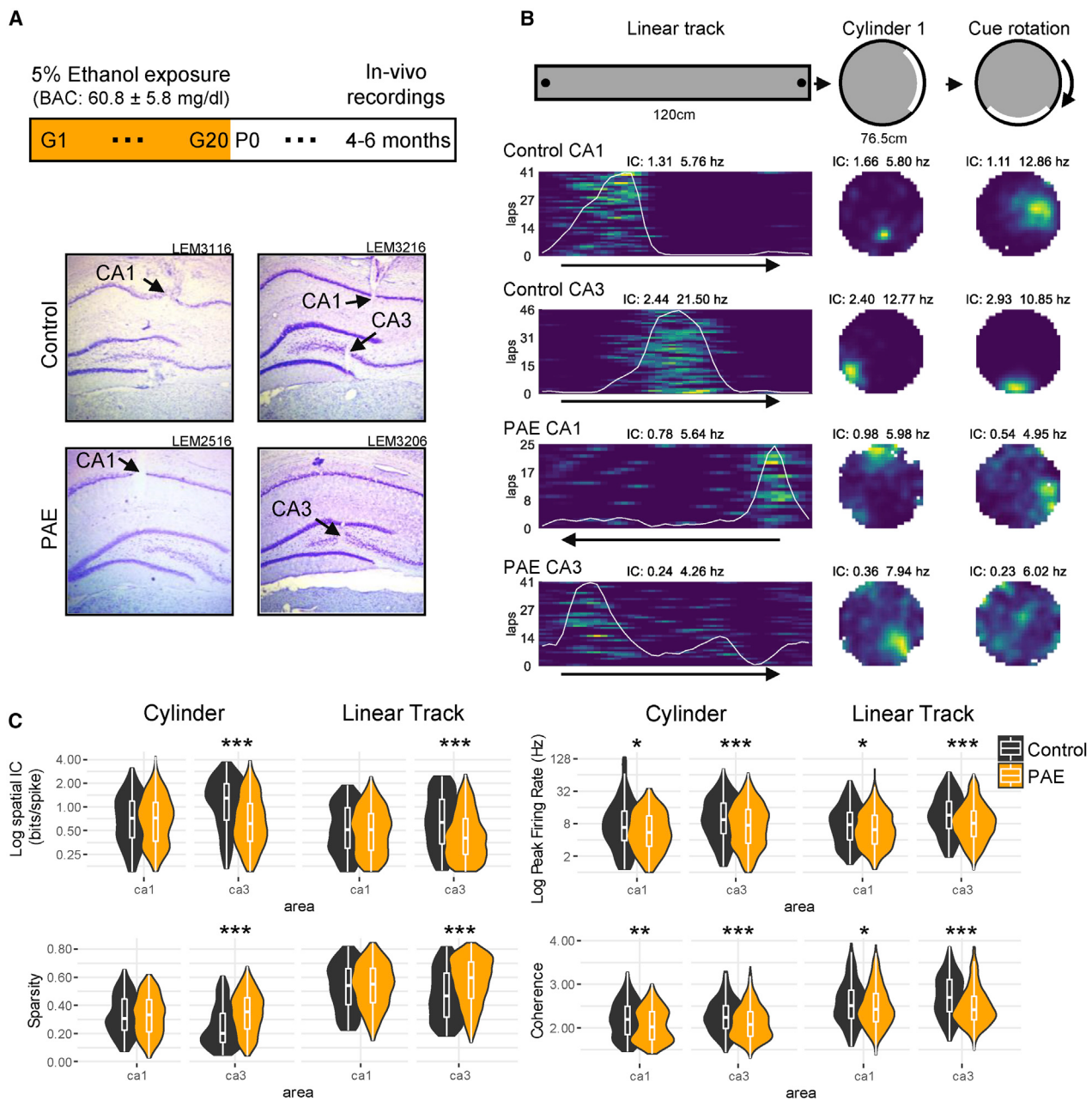


Figure 1. Experimental Protocol, HPC Place Cell Examples, and Group Comparisons

(A) Ethanol exposure paradigm. Top: ethanol exposure and experimental timeline are shown. Bottom: representative Nissl-stained histological images ($4\times$ magnification) show electrode penetration (black arrow) in HPC CA1 and CA3 from control and PAE rats.

(B) Top: environments for assessing HPC place cells. Session 1: 120-cm linear track is shown (black dots indicate reward sites); session 2: 76.5-cm open cylinder with a salient cue (white) is shown; session 3: 67-cm open cylinder with rotated salient cue is shown. Bottom: place cell rate map examples from each group HPC subregion exhibiting spatial firing in all 3 sessions are shown. Spatial information content (IC) and peak firing rate (Hz) are shown above each rate map. Color is scaled with the maximum firing rate for each cell and environment. Running direction on the linear track is shown with a black arrow, and each lap is represented on the y axis.

(C) Violin and boxplots show group comparisons for spatial IC, sparsity, peaking firing rate, and spatial coherence. Violin plots show the distribution density (violin outline) and the appended boxplot box ranges from the 1st (Q1) to the 3rd quartile (Q3), the band inside showing the median, and the extremities of the whiskers showing Q1-1.5*(Q3-Q1) on top and Q3+1.5*(Q3-Q1) on the bottom. * $p < 0.05$; ** $p < 0.01$; *** $p < 0.001$. Average firing rates and bursting properties over sessions are shown in Figure S1.

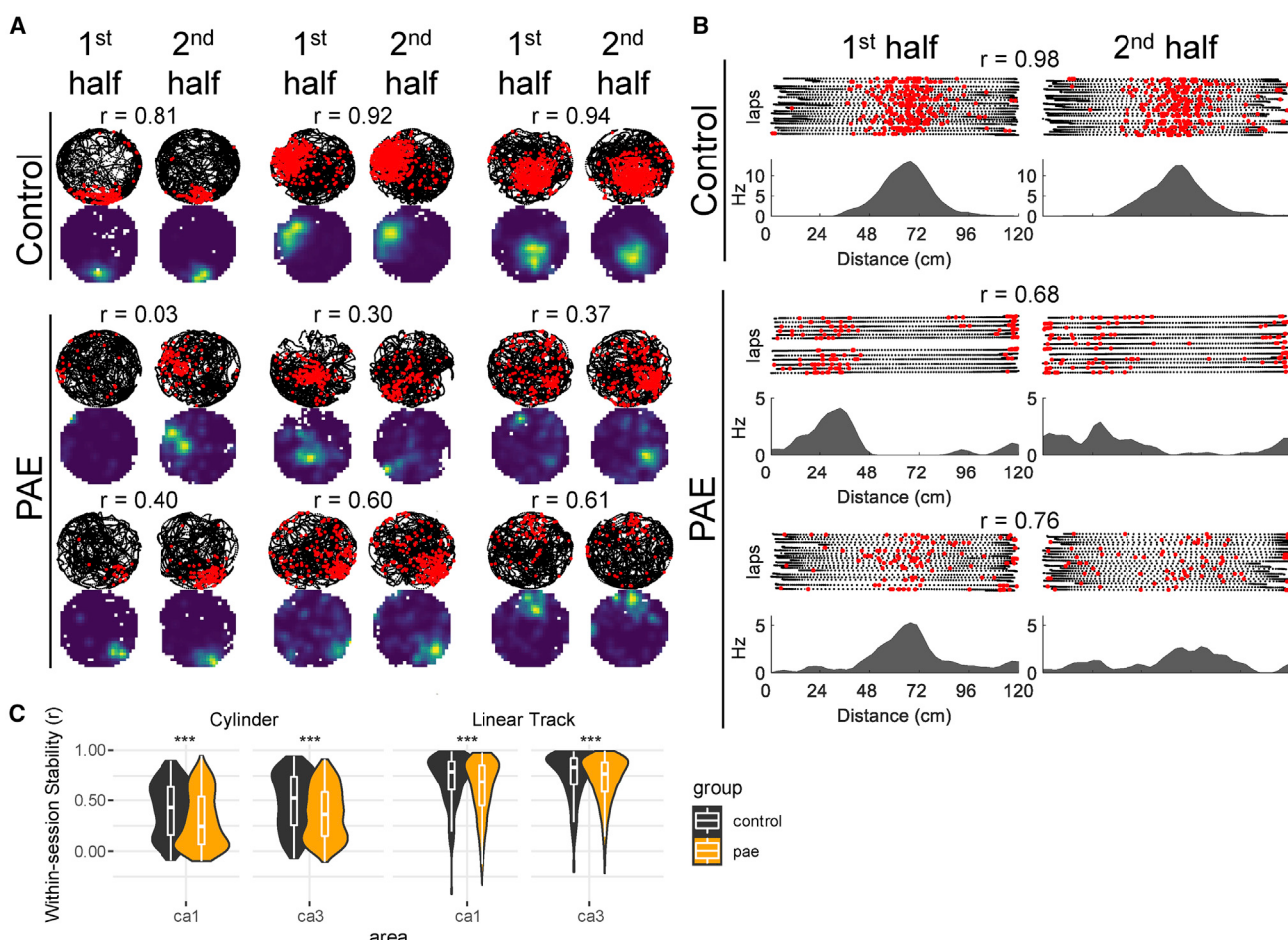


Figure 2. Reduced within-Session Stability by CA1 and CA3 Place Cells after PAE

(A) Control and PAE example place cells from the first and second halves of their respective recording sessions in the cylinder. Note the decreased stability in the PAE group. Rat's path (black dots) and neuron's action potentials (red dots) are shown. Warm colors represent high firing locations. Within-session spatial correlations (r) are shown above each cell.

(B) Control and PAE example place cells from the first and second halves of their respective recording sessions in the linear track.

(C) CA1 and CA3 place cells from PAE rats have reduced spatial correlations (r) between the first and second halves of a recording session in both cylinder and linear track environments (median differences: cylinder CA1 0.19; cylinder CA3 0.16; track CA1 0.10; track CA3 0.06). * $p < 0.05$; ** $p < 0.01$; *** $p < 0.001$. A quantification of behavioral stability can be found in Figure S2.

index between the two running directions was significantly lower for CA3 PAE place cells ($p < 0.001$; WRS; effect size [r] = 0.13; Figures 3A–3D), indicating that CA3 place cells are less likely to orthogonalize their firing rates on the linear track in PAE rats. Together, mechanisms underlying place cell directionality are disrupted, suggesting that rats with PAE are unable to form unique complex representations that aid in the disambiguation of different environmental directions.

Dominant Control by a Proximal Cue over CA1 and CA3 Place Fields after PAE

We next sought to determine the sensitivity of PAE place cells to landmark manipulation by rotating a cue located along the wall of the open-field cylinder environment (Figure 4A). Importantly, we did not disorient rats between sessions so as to not disrupt their internal path integrator, in effect creating a contextual change by inducing a mismatch between the previously experienced and

the rotated cue position [55–58]. A rotational correlation analysis was used to assess the response of place cells following the 90-degree cue rotation by finding the angle at which the two rate maps showed the highest correlation (i.e., rotation angle; Figure 4A) [55, 59–64]. Consistent with previous literature, cells with correlations below a moderate correlation of 0.4 were not used in this analysis, removing 18% of CA1 and 24% of CA3 control cells and 10% of CA1 and 12% of CA3 PAE cells. The average rotation angle of CA1 place cells was significantly different between PAE and control groups ($F(1,216) = 6.46$; $p = 0.01$; Figure 4B), though both groups exhibited angular distributions that significantly clustered around the expected angle of 90 degrees ($V \geq 59.6$; $p \leq 0.02$). Specifically, CA1 control place cells showed an average rotation angle consistent with cue averaging, whereby an intermediate angle between the first and second cue positions was observed ($\theta = 44.8$ degrees; $Z = 4.00$; $p = 0.01$), although CA1 PAE place cells shifted their field locations more closely with the

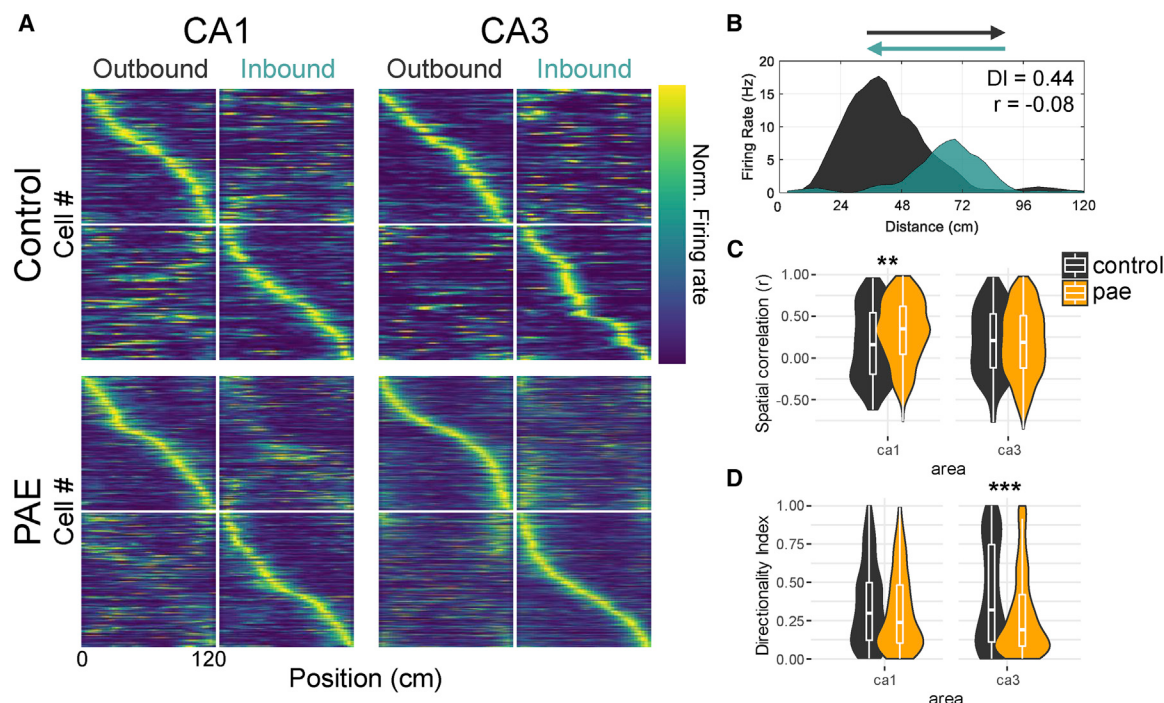


Figure 3. Reduced CA1 and CA3 Place Cell Directionality after PAE

(A) Population vectors of place cells sorted by their location of peak firing rate. Each row (y axis) indicates the firing rate of a single cell as a function of position (x axis). The color indicates firing rate normalized by the peak rate across both running directions for each cell (color bar far right). Note that place cells exhibit increased firing in either outbound or inbound running directions as indicated by the bright diagonal bands. CA1 place cells in PAE rats show a subtle appearance of warmer colors along the diagonal in the opposite running direction.

(B) Example control ca1 place cell on the linear track exemplifying bidirectional coding by both the difference in firing rate (directionality index = 0.44) and in firing position (spatial correlation = -0.08) between the two running directions.

(C) Spatial correlations between rate maps created from the two running directions. Note that PAE CA1 cells are more spatially correlated between the running directions (median CA1 r : control 0.16; PAE 0.35).

(D) Directionality index, a metric of firing rate difference, between the running directions. Note that PAE CA3 cells have decreased directionality index values, indicating that PAE CA3 cells have similar firing rates between the two running directions (median CA3 directionality: control 0.32; PAE 0.19). * $p < 0.05$; ** $p < 0.01$; *** $p < 0.001$.

cue ($\theta = 82.84$ degrees; $Z = 24.38$; $p < 0.001$). Similarly, the rotation angle of CA3 place cells was also significantly different between groups ($F(1,505) = 82.08$; $p < 0.001$). CA3 control place cells had a wider distribution of rotation angles that were not clustered around 90 degrees ($\theta = 246.4$ degrees, $Z = 3.01$, $p = 0.048$; $V = -16.5$, $p = 0.98$). In contrast, CA3 PAE place cells rotated their fields in correspondence with the cue shift ($\theta = 73.2$ degrees, $Z = 31.7$, $p < 0.001$; $V = 107.52$, $p < 0.001$). Overall, both CA1 and CA3 PAE place fields were strongly dominated by the proximal cue within the open field.

Next, we measured the sensitivity of place cell activity in cue manipulation tests by comparing firing rates and spatial tuning across sessions (Figures 4C and 4D). Control cells from CA1 and CA3 demonstrated greater rate remapping between the two sessions compared with PAE cells (CA1: $p < 0.001$, WRS, effect size $[r] = 0.20$; CA3: $p < 0.001$, WRS, effect size $[r] = 0.27$; Figure 4C). Finally, we used difference scores to determine whether changes in spatial tuning between the first and cue-shift cylinder sessions would be similar between control and PAE place cells. Spatial tuning of CA3 place cells between the two sessions was differentially changed compared to control cells (Δ spatial information content: $p < 0.01$, WRS, effect size $[r] = 0.12$; Δ sparsity: $p < 0.05$, WRS, effect size $[r] = 0.09$; Figure 4D). Specifically, control cells displayed

increased variability between the two conditions. Together, the observations suggest that PAE place cells were less likely to exhibit a change in spatial firing and more rigidly represented their environment in accordance with the proximal cue despite rotation.

Place Cell Intrinsic Theta Frequency and Phase Precession Are Disrupted after PAE

Place cells are known to rhythmically fire at theta frequency (4–12 Hz) and demonstrate a phenomenon known as phase precession when an animal passes through its place field [17]. During phase precession, place cells fire at a progressively earlier phase of the local theta rhythms. Therefore, place cells can simultaneously exhibit rate (place) and phase coding, which in effect increases the spatial information contained within any given firing sequence [66]. Thus, we next investigated whether moderate PAE alters the theta rhythmicity and/or phase precession of CA1/CA3 place cells.

Intrinsic Theta Frequency

We first investigated intrinsic theta frequencies using a maximum-likelihood estimation approach [67]. We found that the proportion of significant theta rhythmicity was reduced in PAE CA1 and CA3 place cells in the cylinder session (CA1: $\chi^2 [1, N = 1,691] = 13.92$,

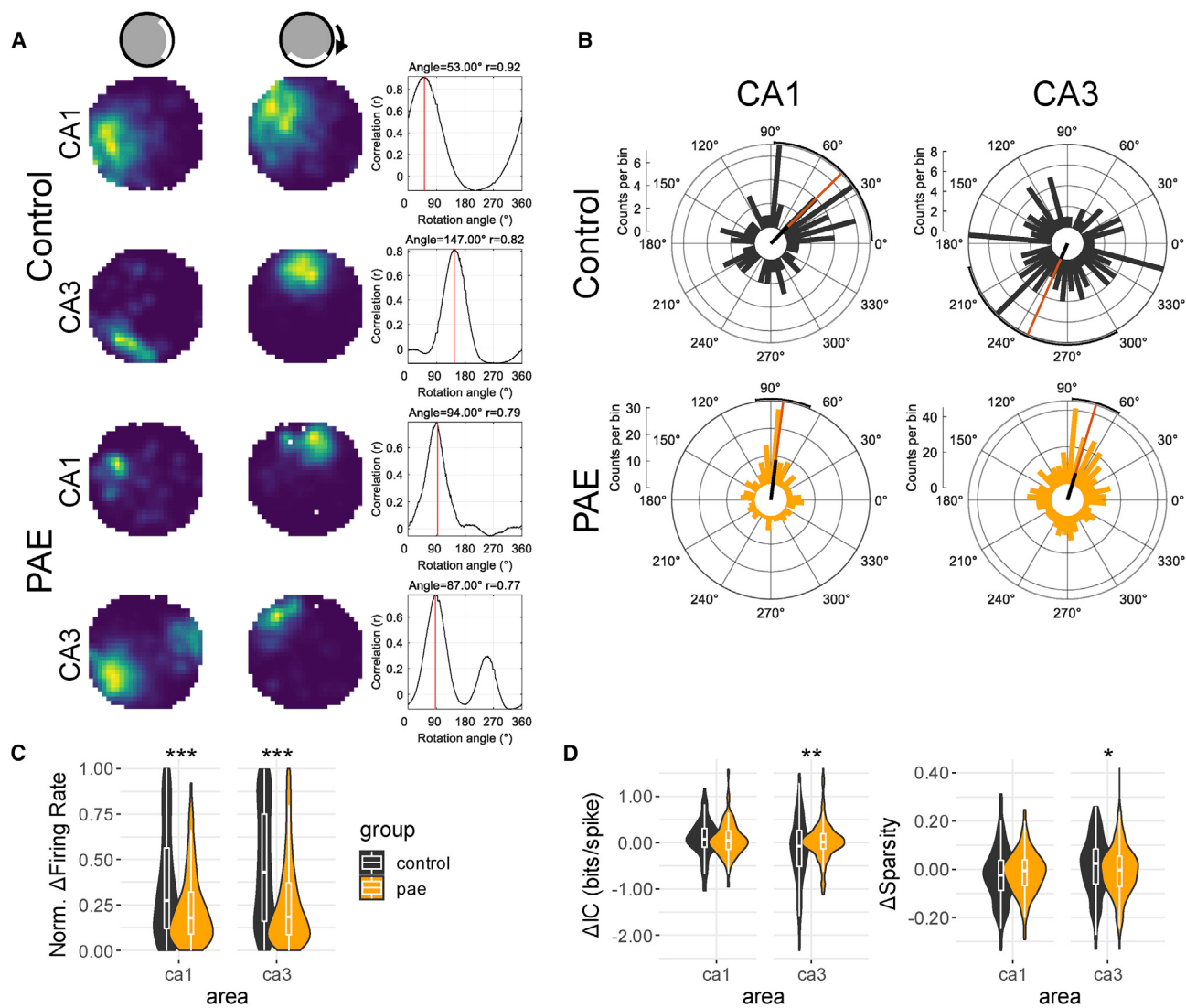


Figure 4. Dominant Control by a Proximal Cue over CA1 and CA3 Place Fields after PAE

(A) Example place cells from standard cylinder session 1 (left) and the cue rotation session (middle). The right panel shows the rotational correlation analysis, where the rate map from the rotation session was rotated in 6-degree bins and a spatial correlation was taken for each correlation. The rotation that resulted in the highest correlation (red line) was assumed to be the directional displacement between the two sessions.

(B) Polar histograms showing the distribution of place field rotation following the cue rotation. Note that although control CA1 and CA3 cells have mostly wide distributions, PAE CA1 and CA3 cells display tight distributions clustered around 90 degrees. The orange bar represents mean direction, and the black bar represents the relative mean vector length of each distribution. Polar plots were created using the CircNNTb MATLAB package [65].

(C) Normalized firing rate difference between cylinder session one and two. Control CA1 and CA3 place cells are more likely to exhibit rate remapping compared with PAE cells.

(D) Change in spatial tuning (spatial information content and sparsity) between cylinder session one and two. Spatial information and sparsity differences scores were created by subtracting values obtained in session 1 from values in session 2. Note the significant group differences in CA3 cell between both spatial tuning metrics (Δ spatial information content: control median = -0.07, PAE median = 0.01; Δ sparsity: control median = 0.02, PAE median = -0.00). * $p < 0.05$; ** $p < 0.01$; *** $p < 0.001$.

$p < 0.001$, effect size [V] = 0.02; CA3: χ^2 [1, N = 1,1,696] = 32.01, $p < 0.001$, effect size [V] = 0.02) and in PAE CA3 place cells on the linear track (χ^2 [1, N = 1,1,646] = 15.55, $p < 0.001$, effect size [V] = 0.01), but not in PAE CA1 cells on the linear track ($p > 0.05$; Figure 5A), suggesting that environmental and task features on the linear track, such as the two fixed-goal sites, may be associated with greater recruitment of theta-rhythmic neurons in CA1.

Additionally, PAE CA1 and CA3 had significantly slower intrinsic theta frequencies in both linear track and cylinder environments ($p < 0.001$; WRS; effect sizes [r] ≥ 0.16 ; Figures 5B–5D).

Speed-Modulated Intrinsic Theta Frequency

Previous research has shown that the intrinsic frequencies throughout the hippocampal formation are modulated by

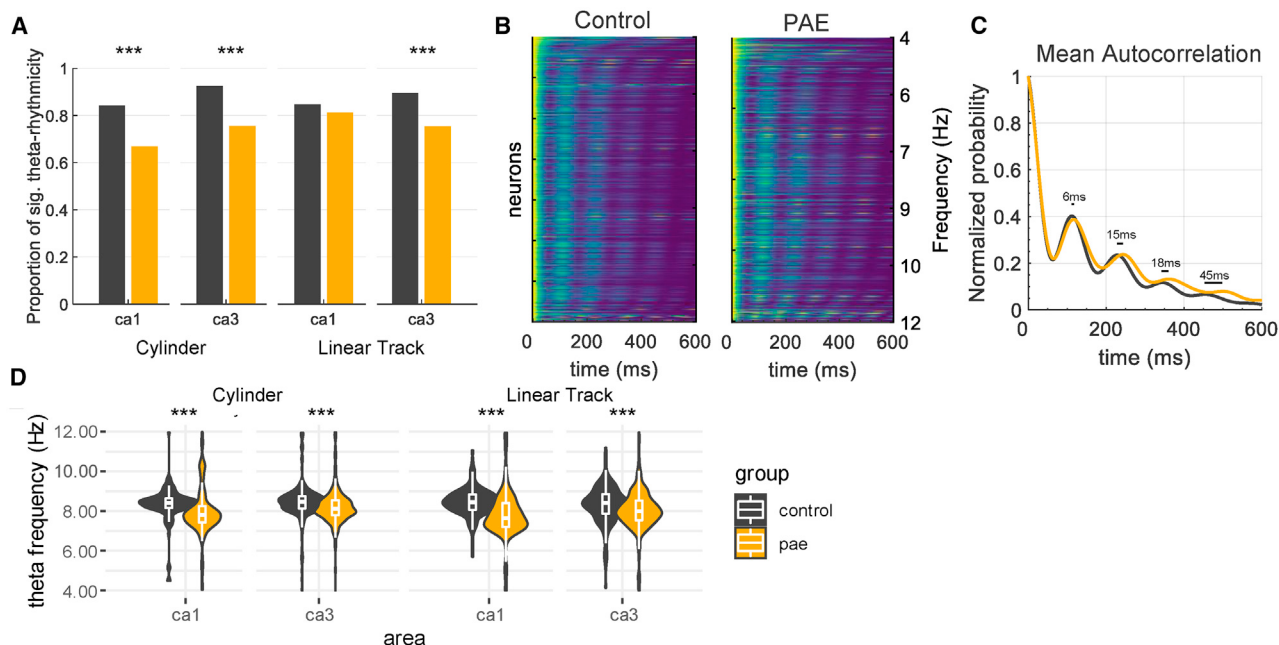


Figure 5. Theta Frequency Is Decreased following PAE

(A) CA1 and CA3 place cells from PAE rats have decreased proportions of significant theta rhythmicity.

(B) Normalized maximum likelihood estimate (MLE) spike-time autocorrelations for control and PAE place cells from CA1 and CA3 and both environments, ordered according to their theta frequency. Warm and cool colors were assigned to the highest and lowest values, respectively, of each autocorrelation.

(C) Mean MLE spike-time correlation fits for all place cells. Note that neurons from the PAE group are approximately 6 ms slower on average for each theta cycle. All theta rhythmic units are shown in Figure S3.

(D) PAE rats have significantly slower spike-time theta frequency across CA1 and CA3 in both linear track and cylinder environments. Median differences: cylinder CA1: 0.61 Hz; cylinder CA3: 0.35 Hz; track CA1: 0.79 Hz; track CA3: 0.42 Hz. *p < 0.05; **p < 0.01; ***p < 0.001.

running speed (example in Figure 6B, right) [51, 68–73]. To take speed modulation into account, we first established that both groups have similar trial average running speeds in both environments (Figure 6A). Next, we computed the intrinsic frequency, again using the maximum likelihood estimation approach [67], during epochs of fast (upper 50%) and slow (lower 50%) running speeds (example in Figure 6B). Running speed differences between slow and fast epochs were similar between groups, and the magnitude of speed differences between high and low running speeds was not predictive of the magnitude of theta frequency difference in either group (Figure S4). However, the frequency shift between the two speeds was significantly larger for control cells compared to the PAE cells ($p < 0.006$; WRS; Figure 6C). To follow up on this finding, we investigated the proportion of theta rhythmic neurons with significantly speed-modulated intrinsic frequencies. We found that running speed was a significant covariate for theta frequency in a greater proportion of CA1 and CA3 control cells in the cylinder and CA1 control cells in the track compared to PAE cells (Figure 6D). Because firing rates of HPC cells have also been found to be modulated running speed [41, 70, 74–82], we investigated whether PAE affected this modulation. Despite having decreased speed-modulated theta frequency, speed-modulated firing rates were unaffected by PAE (Figure S5). Together, intrinsic theta frequency from PAE rats was less modulated by running speed compared to control rats.

Theta Phase Precession

Next, we investigated whether PAE place cells exhibited similar phase precession (Figures 7A–7D). Although the strength of theta-phase precession was similar between groups in both environments, measured by a circular-linear correlation ($p > 0.09$; WRS; Figure 7E), the proportion of individual cells that demonstrated phase precession was significantly reduced in CA3 from PAE rats on the linear track ($\chi^2 [1, N = 1,269] = 4.32$; $p = 0.03$; effect size [V] = 0.05) and in the cylinder ($\chi^2 [1, N = 1,301] = 14.44$; $p < 0.001$; effect size [V] = 0.01; Figure 7F). This latter finding suggests that the specific mechanisms underlying CA3 phase precession may be altered following PAE, although mechanisms underlying CA1 phase precession are spared.

DISCUSSION

The present study established six specific findings regarding the impact of moderate PAE on HPC place cell firing and theta rhythmicity. First, although moderate PAE reduced the consistency of spiking and peak firing rates of place fields across both CA1 and CA3 subregions, the spatial tuning of place fields was disrupted only in CA3. Second, we found that moderate PAE impaired the within-session stability of HPC place fields in both CA1 and CA3 regions. Third, moderate PAE disrupted the directionality of CA1 and CA3 place cells on the linear track. Fourth, CA1 and CA3 place fields in PAE animals showed greater control by a proximal

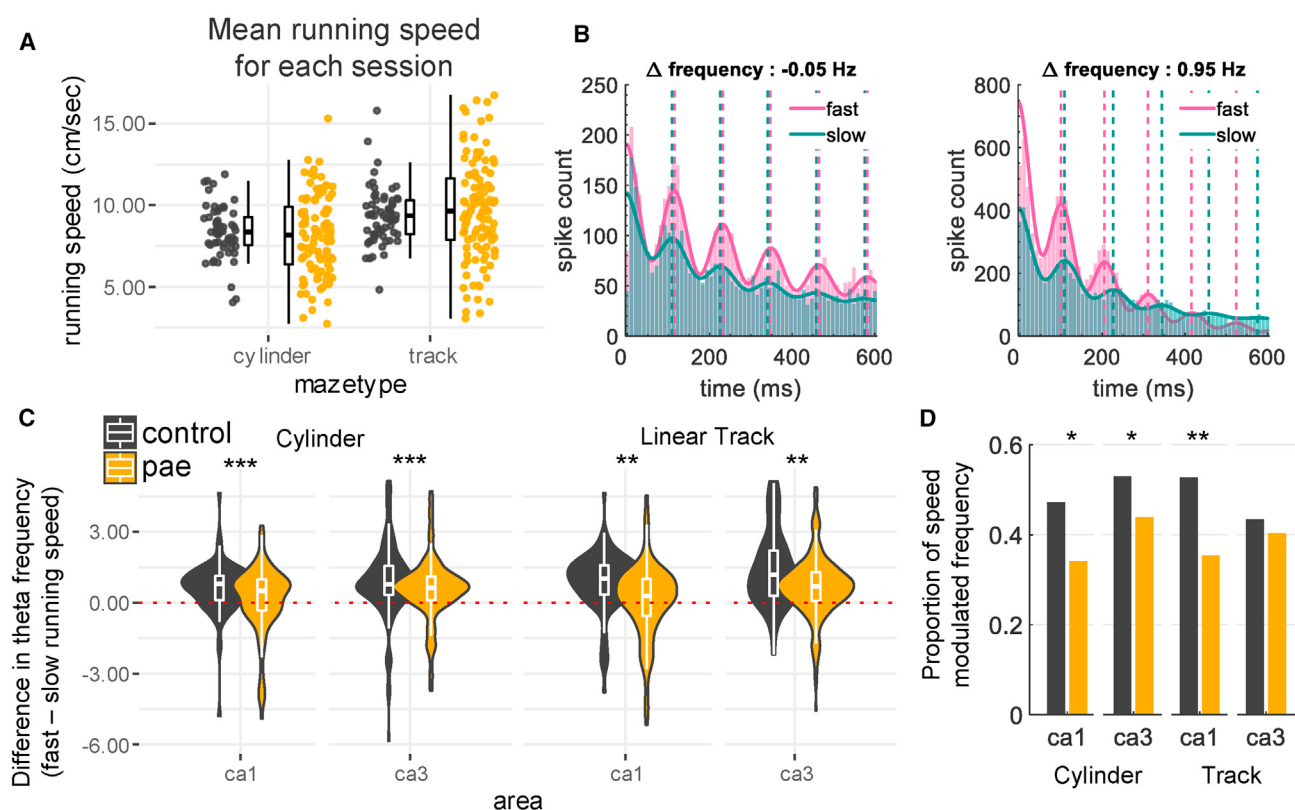


Figure 6. Running-Speed-Dependent Theta Frequency

(A) Mean running speed (cm/s) for each session is similar between control and PAE rats (median speeds: control cylinder = 8.35 cm/s; PAE cylinder = 8.17 cm/s; control track = 9.36 cm/s; PAE track = 9.65 cm/s).

(B) Example cells demonstrating speed-modulated theta rhythmicity. Left: autocorrelogram of spike times using all spikes in the 50% fastest (mean speed 19 cm/s) and 50% slowest (mean speed 4 cm/s) running epochs. Note that this cell lacks intrinsic theta frequency speed modulation, which is evident in the overlapping peaks between the running speeds. This example neuron was from a PAE rat recorded from CA3 while the rat foraged in the cylinder. Right: autocorrelogram of spike times using all spikes in the 50% fastest (mean speed 26 cm/s) and 50% slowest (mean speed 9 cm/s) running epochs is shown. Note that this cell does display intrinsic theta frequency speed modulation, as the fast runs have an increased intrinsic frequency compared to the slow runs. This example neuron was from a control rat recorded from CA3 while the rat foraged in the cylinder. Dotted lines indicate the local maxima for each autocorrelogram, and the frequency differences are displayed above each plot.

(C) Control cells have a larger increase in theta frequency from slow to fast runs compared to PAE cells (medians group differences: CA1 cylinder 0.29; CA3 cylinder 0.14; CA1 track 0.73; CA3 track 0.50).

(D) Running speed is a significant covariate for theta frequency in a greater proportion of CA1 and CA3 control cells in the cylinder and CA1 control cells in the track compared to PAE cells (cylinder CA1 control: 47%, PAE: 34%; cylinder CA3 control: 53%, PAE: 44%; track CA1 control: 53%, PAE: 35%; track CA3 control: 43%, PAE: 40%). * $p < 0.05$; ** $p < 0.01$; *** $p < 0.001$. The relationship between the difference in running speed and theta frequency is shown in Figure S4. Also see Figure S5.

cue. Fifth, we found that PAE slowed intrinsic theta frequencies among CA1 and CA3 place cells, reduced the number of place cells expressing significant theta modulation in the cylinder environment, and decreased speed modulation of theta frequency. Finally, PAE reduced the number of place cells exhibiting significant theta-phase precession in CA3.

Deficits in spatial tuning, stability, and directionality of PAE place cells are likely associated with the observed deficits in HPC excitatory signaling at dentate gyrus synapses following PAE. For instance, moderate PAE has been consistently linked to impairments in synaptic plasticity at perforant pathway-dentate gyrus synapses, even well into adulthood [27–29, 83, 84]. Moreover, a previous study has shown that NMDA subunit composition can be altered in the dentate gyrus of adult mice after moderate PAE [27]. Rate remapping by

CA3 place cells, which was reduced in the present study, is dependent on the integrity of synaptic plasticity and NMDA receptor function at perforant pathway synapses [37]. Previous studies have also reported that moderate PAE can reduce mGluR5 receptor function in the dentate gyrus [85] and leads to elevated histamine H3-receptor-mediated inhibition of glutamate release from perforant path nerve terminals [86]. Likewise, the integrity of input from the entorhinal cortex, which forms the most prominent source of perforant path axons, is critical for place cell activity [87], and damage to entorhinal cortical cells can produce a similar loss of place field stability and reduction in spatial tuning [88–90]. CA1 place cells also receive direct input from layer III entorhinal cells, but this input is not known to have a strong influence on place cell remapping [89], and damage to this projection produces

Current Biology

Article

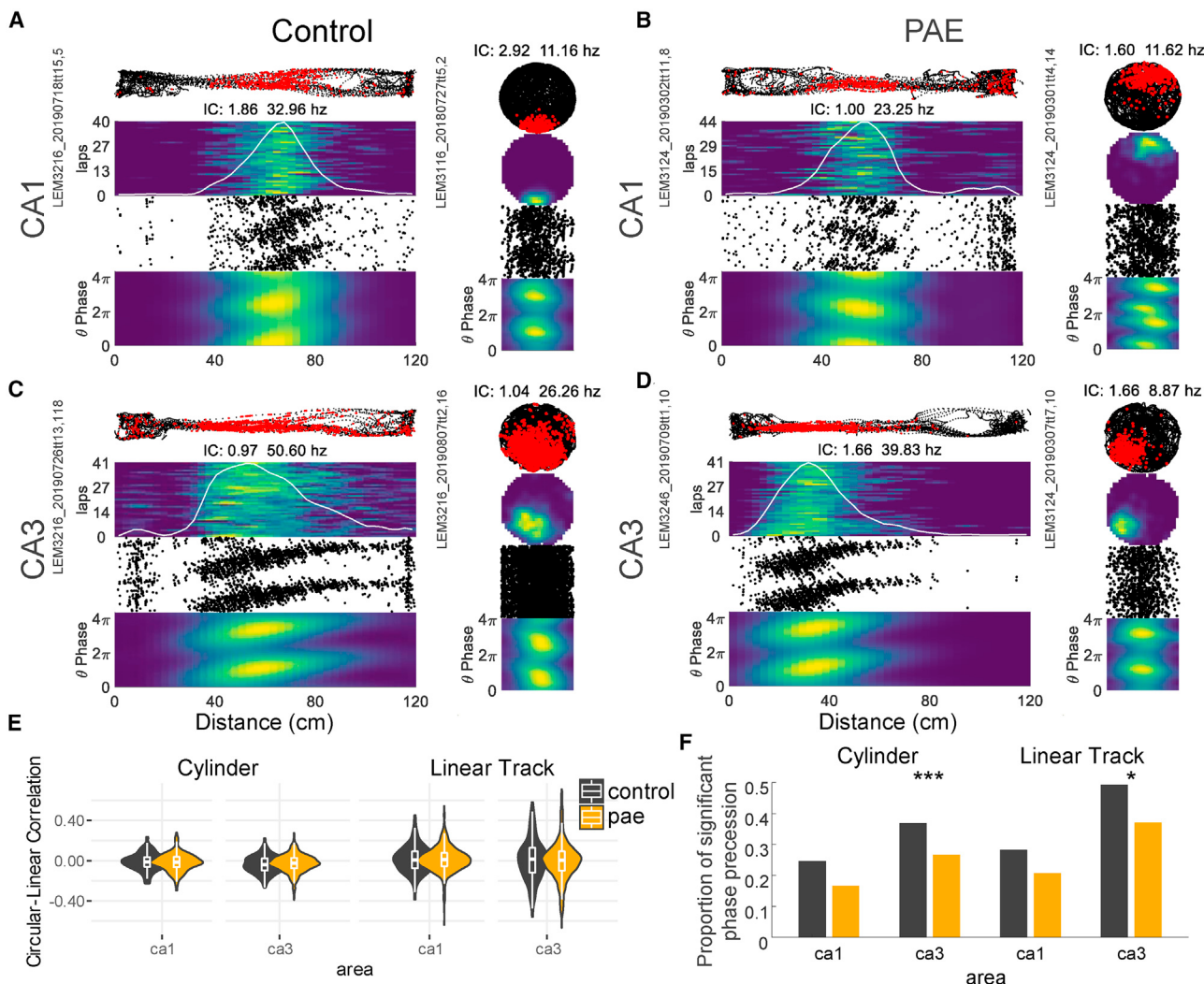


Figure 7. CA3 Theta Phase Precession Is Affected by PAE

(A–D) Each panel shows an example place cell demonstrating significant theta-phase precession from control (CA1: A; CA3: C) and PAE (CA1: B; CA3: D) groups in both environments. Row 1: rat's path (black dots) and neuron's action potentials (red dots) are shown. Row 2: rate maps for each lap for the linear track or overall maps for the cylinder are shown. Warm colors represent high firing locations. The white line represents the mean firing rate across laps for the linear track examples. Spatial IC and peak firing rate are listed at the top of each example cell. Row 3: distance by theta-phase scatterplots is shown. Row 4: distance by theta-phase rate maps is shown.

(E) Circular-linear correlations. Control and PAE place cells had similar circular-linear correlations in both brain regions and both environments.

(F) The proportion of cells demonstrating significant theta phase precession. PAE CA3 place cells had significantly reduced proportions of phase precession in both environments (group differences: cylinder 0.10; track 0.12). *p < 0.05; **p < 0.01; ***p < 0.001.

reductions in the spatial tuning of CA1 place cells [91], which was not observed in the present study.

We also found that HPC place cells recorded in the PAE group were preferentially controlled by a cue located along the wall of the cylinder environment. Specifically, when the proximal cue was rotated by 90 degrees, a large majority of place cells recorded in the PAE group rotated their firing fields in the same angular direction and distance as the cue. In control subjects, place cells were less likely to rotate their firing fields with the cue but instead demonstrated cue averaging (i.e., partial angular rotation) or "remapping" of their firing fields to largely random locations. The findings support the conclusion that HPC circuitry in

PAE animals can establish strong associations with proximal cues, but sensitivity to other contextual stimuli, such as distal visual cues, appears more limited. For instance, between cylinder tests (standard and rotation), animals were carefully transported to and from a resting pedestal between sessions with full access to available visual cues in the recording room. Thus, stimuli marking the global frame of reference and self-motion cues (e.g., vestibular, motor, etc.) remained intact between cylinder sessions. Providing rats with access to visual cues during cue rotations has shown to disrupt cue control, whereby place fields may shift out of sync with the degree of the cue shift [57, 58]. Furthermore, place fields are also influenced by distal- and

self-motion-based cues [57, 61, 92, 93], and the conflict between these and the proximal cue rotation may have induced place field remapping in the control group. Indeed, evidence of proximal cue influence in the form of cue averaging was observed for fields in CA1 of the control group (see Figure 4B). Thus, a weakened capacity to establish associations with distal and/or self-motion cues may be a consequence of moderate PAE. Previous research suggests that information regarding the distal framework and self-motion cues is largely derived from medial entorhinal cortex input to the hippocampus and indirect sources from other parahippocampal regions [94–96]. As already noted above, perforant path input to the dentate gyrus is weakened in moderate PAE. However, whether deficits are preferential to the medial perforant pathway has not been systematically investigated after moderate PAE. A final point is that an enhancement in proximal cue control may also explain the observed reduction in place field directionality in the PAE group. Previous work has reported a similar finding when proximal cues were placed along the surface of a linear track, thereby enhancing the salience of the proximal frame of reference [39].

Several of the present results parallel spatial behavior deficits previously reported in human fetal alcohol spectrum disorder (FASD) and animal models of PAE. Specifically, we found that PAE place cells were less likely to orthogonalize their firing in opposite directions of travel. This inflexibility in place cell representation could explain previous reports of poor spatial discrimination by PAE animals in tasks utilizing narrow maze arms [21, 22]. The rigidity of place cell firing on the linear track may be extended to explain deficits in tasks requiring PAE animals to rapidly learn a new spatial location in open environments, such as the Morris water task [9, 18, 19]. We also found that PAE place cells expressed reductions in spatial tuning specifically in CA3 and subtle field instability across 20- to 30-min recording sessions in both HPC subregions. Previous studies have found that reductions in place field tuning and stability are associated with spatial learning and memory deficits [97, 98]. Thus, similar findings would be expected, in which reductions in spatial tuning, stability, and directionality would predict spatial learning and memory deficits observed after moderate PAE. Future work should be designed to test this hypothesis. In contrast to deficits in spatial learning after PAE, tests in the Morris water task with PAE rats have reported a preference for navigation to spatial locations marked by a local cue as opposed to navigation based on distal cues [9]. Similar observations have been reported in tests of virtual navigation by children with FASD [99]. These findings of intact cue-based navigation parallel our observation of dominant control by a proximal landmark over PAE place fields. We have speculated that the results of the present study, when taken together with prior spatial behavioral results, point to a functional loss in the neural systems involved in processing distal and/or self-motion cues while leaving the proximal frame of reference intact. Tests of this hypothesis will require that future studies combine systematic manipulation of distal, self-motion, and proximal cues with behavior and simultaneous multi-site recordings from neural circuits involved in these processes [100].

Along with changes in place cell rate coding after moderate PAE, we also identified alterations in place cell theta rhythmicity. We first found a smaller proportion of PAE CA1 and CA3 place

cells modulated by the theta frequency. Second, those that were theta rhythmic had reduced intrinsic theta frequency as well as decreased running speed modulation compared with control cells. Likewise, this decrease was paralleled with a subtle decrease in firing rates of place cells from PAE rats. This alteration in theta frequency may partially explain previously reported spatial deficits in rodents with PAE (reviewed in [7]), as the integrity of HPC theta oscillations has been linked to accurate spatial memory [16, 101]. Disruption of HPC phase precession has been linked to spatial memory impairments [102, 103]. Additionally, phase locking of HPC spiking to particular local field potential theta phases, although not investigated here, has been associated with learning in HPC-dependent tasks [104]. Recent evidence suggests that moderate PAE reduces the number of fast-spiking parvalbumin+GABAergic interneurons throughout the HPC [105]. Importantly, these interneurons play a vital role in regulating theta-phase precession and HPC theta rhythms [106–108]. Consequently, the reduction of theta frequency may be associated with microcircuit changes as a result of the reduced number of GABAergic interneurons. Future studies are needed to determine whether HPC microcircuit function is substantially altered by PAE, which would result in theta-frequency reductions. Whether other HPC oscillations (e.g., gamma- or sharp-wave ripples) are disrupted after PAE is currently unknown and should also be investigated in future studies.

To summarize, the present study establishes a clear linkage between moderate PAE and deficits in spatial and rhythmic firing by HPC cell populations. We are unaware of previous work investigating the developmental impact of alcohol on HPC place cell activity. Additionally, although structural changes to the hippocampus and deficits in HPC-dependent behavior have been established after moderate PAE, changes at the level of neural population activity *in vivo* have not received similar systematic investigation. Thus, the findings of the present study represent a critical step in developing a complete multi-level understanding of the neurobiological basis of spatial learning and memory impairments after moderate PAE.

STAR★METHODS

Detailed methods are provided in the online version of this paper and include the following:

- **KEY RESOURCES TABLE**
- **RESOURCE AVAILABILITY**
 - Lead Contact
 - Materials Availability
 - Data and Code Availability
- **EXPERIMENTAL MODEL AND SUBJECT DETAILS**
 - Subjects
 - Breeding and voluntary ethanol consumption
- **METHOD DETAILS**
 - Surgical procedures
 - Apparatus
 - Behavioral training
 - Recording Procedures
 - Histology
 - Spike sorting
 - Spatial rate map construction

Current Biology

Article



- Spatial information
- Sparsity
- Spatial correlation
- Spatial coherence
- Directionality Index
- Place cell classification
- Cue rotation analysis
- Instantaneous theta phase, firing phase
- Theta phase precession
- Spike-train theta rhythmicity
- Speed modulated cells
- QUANTIFICATION AND STATISTICAL ANALYSIS
 - Data analysis
 - Statistical Analysis

SUPPLEMENTAL INFORMATION

Supplemental Information can be found online at <https://doi.org/10.1016/j.cub.2020.06.077>.

ACKNOWLEDGMENTS

The authors thank Dr. Suzy Davies and Dr. Jennifer Wagner for supervising the moderate PAE paradigm and Andre Moezzi, Nicole Graham, Kiana Lujan, Ella Rappaport, and Chloe Puglisi for their assistance with the rodent husbandry procedures. The research reported in this publication was supported by National Institute on Alcohol Abuse and Alcoholism grants R21 AA024983, P50 AA022534, and T32 AA014127-15.

AUTHOR CONTRIBUTIONS

R.E.H., D.D.S., D.A.H., and B.J.C. conceptualized experiments. B.J.C. contributed lab resources and supervision. D.D.S. created the animal model and directed the production of experimental offspring. R.E.H. and L.E.B. collected and analyzed data with input from B.J.C. R.E.H., L.E.B., and B.J.C. wrote the initial draft of the paper with D.D.S. and D.A.H. providing review and editing.

DECLARATION OF INTERESTS

The authors declare no competing interests.

Received: February 22, 2020

Revised: May 26, 2020

Accepted: June 23, 2020

Published: July 23, 2020

REFERENCES

1. Guerri, C., and Sanchis, R. (1985). Acetaldehyde and alcohol levels in pregnant rats and their fetuses. *Alcohol* 2, 267–270.
2. Day, N.L., Leech, S.L., Richardson, G.A., Cornelius, M.D., Robles, N., and Larkby, C. (2002). Prenatal alcohol exposure predicts continued deficits in offspring size at 14 years of age. *Alcohol. Clin. Exp. Res.* 26, 1584–1591.
3. Green, C.R., Mihic, A.M., Nikkel, S.M., Stade, B.C., Rasmussen, C., Munoz, D.P., and Reynolds, J.N. (2009). Executive function deficits in children with fetal alcohol spectrum disorders (FASD) measured using the Cambridge Neuropsychological Tests Automated Battery (CANTAB). *J. Child Psychol. Psychiatry* 50, 688–697.
4. Thomas, S.E., Kelly, S.J., Mattson, S.N., and Riley, E.P. (1998). Comparison of social abilities of children with fetal alcohol syndrome to those of children with similar IQ scores and normal controls. *Alcohol. Clin. Exp. Res.* 22, 528–533.
5. Popova, S., Lange, S., Probst, C., Gmel, G., and Rehm, J. (2017). Estimation of national, regional, and global prevalence of alcohol use during pregnancy and fetal alcohol syndrome: a systematic review and meta-analysis. *Lancet Glob. Health* 5, e290–e299.
6. Berman, R.F., and Hannigan, J.H. (2000). Effects of prenatal alcohol exposure on the hippocampus: spatial behavior, electrophysiology, and neuroanatomy. *Hippocampus* 10, 94–110.
7. Harvey, R.E., Berkowitz, L.E., Hamilton, D.A., and Clark, B.J. (2019). The effects of developmental alcohol exposure on the neurobiology of spatial processing. *Neurosci. Biobehav. Rev.* 107, 775–794.
8. Mira, R.G., Lira, M., Tapia-Rojas, C., Rebollo, D.L., Quintanilla, R.A., and Cerpa, W. (2020). Effect of alcohol on hippocampal-dependent plasticity and behavior: role of glutamatergic synaptic transmission. *Front. Behav. Neurosci.* 13, 288.
9. Sutherland, R.J., McDonald, R.J., and Savage, D.D. (2000). Prenatal exposure to moderate levels of ethanol can have long-lasting effects on learning and memory in adult offspring. *Psychobiology* 28, 532–539.
10. Valenzuela, C.F., Morton, R.A., Diaz, M.R., and Topper, L. (2012). Does moderate drinking harm the fetal brain? Insights from animal models. *Trends Neurosci.* 35, 284–292.
11. Morris, R.G.M., Garrud, P., Rawlins, J.N.P., and O'Keefe, J. (1982). Place navigation impaired in rats with hippocampal lesions. *Nature* 297, 681–683.
12. Eichenbaum, H., Yonelinas, A.P., and Ranganath, C. (2007). The medial temporal lobe and recognition memory. *Annu. Rev. Neurosci.* 30, 123–152.
13. Scoville, W.B., and Milner, B. (1957). Loss of recent memory after bilateral hippocampal lesions. *J. Neurol. Neurosurg. Psychiatry* 20, 11–21.
14. O'Keefe, J. (1976). Place units in the hippocampus of the freely moving rat. *Exp. Neurol.* 51, 78–109.
15. O'Keefe, J., and Burgess, N. (2005). The hippocampus as a spatial map: Preliminary evidence from unit activity in the freely-moving rat. *Brain Res.* 34, 171–175.
16. O'Keefe, J., and Burgess, N. (2007). The Hippocampus as a Cognitive Map (Clarendon).
17. O'Keefe, J., and Burgess, N. (2009). Phase relationship between hippocampal place units and the EEG theta rhythm. *Hippocampus* 3, 317–330.
18. Hamilton, D.A., Barto, D., Rodriguez, C.I., Magcalas, C.M., Fink, B.C., Rice, J.P., Bird, C.W., Davies, S., and Savage, D.D. (2014). Effects of moderate prenatal ethanol exposure and age on social behavior, spatial response perseveration errors and motor behavior. *Behav. Brain Res.* 269, 44–54.
19. Rodriguez, C.I., Magcalas, C.M., Barto, D., Fink, B.C., Rice, J.P., Bird, C.W., Davies, S., Pentkowski, N.S., Savage, D.D., and Hamilton, D.A. (2016). Effects of sex and housing on social, spatial, and motor behavior in adult rats exposed to moderate levels of alcohol during prenatal development. *Behav. Brain Res.* 313, 233–243.
20. Savage, D.D., Becher, M., de la Torre, A.J., and Sutherland, R.J. (2002). Dose-dependent effects of prenatal ethanol exposure on synaptic plasticity and learning in mature offspring. *Alcohol. Clin. Exp. Res.* 26, 1752–1758.
21. Brady, M.L., Allan, A.M., and Caldwell, K.K. (2012). A limited access mouse model of prenatal alcohol exposure that produces long-lasting deficits in hippocampal-dependent learning and memory. *Alcohol. Clin. Exp. Res.* 36, 457–466.
22. Sanchez, L.M., Goss, J., Wagner, J., Davies, S., Savage, D.D., Hamilton, D.A., and Clark, B.J. (2019). Moderate prenatal alcohol exposure impairs performance by adult male rats in an object-place paired-associate task. *Behav. Brain Res.* 360, 228–234.
23. Behrens, T.E.J., Muller, T.H., Whittington, J.C.R., Mark, S., Baram, A.B., Stachenfeld, K.L., and Kurth-Nelson, Z. (2018). What is a cognitive map? Organizing knowledge for flexible behavior. *Neuron* 100, 490–509.
24. Rubin, A., Yartsev, M.M., and Ulanovsky, N. (2014). Encoding of head direction by hippocampal place cells in bats. *J. Neurosci.* 34, 1067–1080.

25. Bliss, T.V., and Lomo, T. (1973). Long-lasting potentiation of synaptic transmission in the dentate area of the anaesthetized rabbit following stimulation of the perforant path. *J. Physiol.* 232, 331–356.
26. McNaughton, B.L., and Morris, R.G.M. (1987). Hippocampal synaptic enhancement and information storage within a distributed memory system. *Trends Neurosci.* 10, 408–415.
27. Brady, M.L., Diaz, M.R., Iuso, A., Everett, J.C., Valenzuela, C.F., and Caldwell, K.K. (2013). Moderate prenatal alcohol exposure reduces plasticity and alters NMDA receptor subunit composition in the dentate gyrus. *J. Neurosci.* 33, 1062–1067.
28. Sutherland, R.J., McDonald, R.J., and Savage, D.D. (1997). Prenatal exposure to moderate levels of ethanol can have long-lasting effects on hippocampal synaptic plasticity in adult offspring. *Hippocampus* 7, 232–238.
29. Varaschin, R.K., Akers, K.G., Rosenberg, M.J., Hamilton, D.A., and Savage, D.D. (2010). Effects of the cognition-enhancing agent ABT-239 on fetal ethanol-induced deficits in dentate gyrus synaptic plasticity. *J. Pharmacol. Exp. Ther.* 334, 191–198.
30. Agnihotri, N.T., Hawkins, R.D., Kandel, E.R., and Kentros, C. (2004). The long-term stability of new hippocampal place fields requires new protein synthesis. *Proc. Natl. Acad. Sci. USA* 101, 3656–3661.
31. Barnes, C.A. (1979). Memory deficits associated with senescence: a neurophysiological and behavioral study in the rat. *J. Comp. Physiol. Psychol.* 93, 74–104.
32. Barnes, C.A., and McNaughton, B.L. (1980). Physiological compensation for loss of afferent synapses in rat hippocampal granule cells during senescence. *J. Physiol.* 309, 473–485.
33. Barnes, C.A., Rao, G., and Houston, F.P. (2000). LTP induction threshold change in old rats at the perforant path–granule cell synapse. *Neurobiol. Aging* 21, 613–620.
34. Dieguez, D., Jr., and Barea-Rodriguez, E.J. (2004). Aging impairs the late phase of long-term potentiation at the medial perforant path–CA3 synapse in awake rats. *Synapse* 52, 53–61.
35. Rotenberg, A., Mayford, M., Hawkins, R.D., Kandel, E.R., and Muller, R.U. (1996). Mice expressing activated CaMKII lack low frequency LTP and do not form stable place cells in the CA1 region of the hippocampus. *Cell* 87, 1351–1361.
36. Rotenberg, A., Abel, T., Hawkins, R.D., Kandel, E.R., and Muller, R.U. (2000). Parallel instabilities of long-term potentiation, place cells, and learning caused by decreased protein kinase A activity. *J. Neurosci.* 20, 8096–8102.
37. McHugh, T.J., Jones, M.W., Quinn, J.J., Balthasar, N., Coppari, R., Elmquist, J.K., Lowell, B.B., Fanselow, M.S., Wilson, M.A., and Tonegawa, S. (2007). Dentate gyrus NMDA receptors mediate rapid pattern separation in the hippocampal network. *Science* 317, 94–99.
38. Yassa, M.A., and Stark, C.E. (2011). Pattern separation in the hippocampus. *Trends Neurosci.* 34, 515–525.
39. Battaglia, F.P., Sutherland, G.R., and McNaughton, B.L. (2004). Local sensory cues and place cell directionality: additional evidence of prospective coding in the hippocampus. *J. Neurosci.* 24, 4541–4550.
40. Frank, L.M., Stanley, G.B., and Brown, E.N. (2004). Hippocampal plasticity across multiple days of exposure to novel environments. *J. Neurosci.* 24, 7681–7689.
41. McNaughton, B.L., Barnes, C.A., and O'Keefe, J. (1983). The contributions of position, direction, and velocity to single unit activity in the hippocampus of freely-moving rats. *Exp. Brain Res.* 52, 41–49.
42. Matthews, D.B., Simson, P.E., and Best, P.J. (1996). Ethanol alters spatial processing of hippocampal place cells: a mechanism for impaired navigation when intoxicated. *Alcohol. Clin. Exp. Res.* 20, 404–407.
43. White, A.M., and Best, P.J. (2000). Effects of ethanol on hippocampal place-cell and interneuron activity. *Brain Res.* 876, 154–165.
44. Davies, S., Ballesteros-Merino, C., Allen, N.A., Porch, M.W., Pruitt, M.E., Christensen, K.H., Rosenberg, M.J., and Savage, D.D. (2019). Impact of moderate prenatal alcohol exposure on histaminergic neurons, histidine decarboxylase levels and histamine H₂ receptors in adult rat offspring. *Alcohol* 76, 47–57.
45. Lee, I., Yoganarasimha, D., Rao, G., and Knierim, J.J. (2004). Comparison of population coherence of place cells in hippocampal sub-fields CA1 and CA3. *Nature* 430, 456–459.
46. Leutgeb, S., Leutgeb, J.K., Treves, A., Moser, M.B., and Moser, E.I. (2004). Distinct ensemble codes in hippocampal areas CA3 and CA1. *Science* 305, 1295–1298.
47. Park, E., Dvorak, D., and Fenton, A.A. (2011). Ensemble place codes in hippocampus: CA1, CA3, and dentate gyrus place cells have multiple place fields in large environments. *PLoS ONE* 6, e22349.
48. Roth, E.D., Yu, X., Rao, G., and Knierim, J.J. (2012). Functional differences in the backward shifts of CA1 and CA3 place fields in novel and familiar environments. *PLoS ONE* 7, e36035.
49. Mizuseki, K., Royer, S., Diba, K., and Buzsáki, G. (2012). Activity dynamics and behavioral correlates of CA3 and CA1 hippocampal pyramidal neurons. *Hippocampus* 22, 1659–1680.
50. Patten, A.R., Sawchuk, S., Wortman, R.C., Brocardo, P.S., Gil-Mohapel, J., and Christie, B.R. (2016). Prenatal ethanol exposure impairs temporal ordering behaviours in young adult rats. *Behav. Brain Res.* 299, 81–89.
51. Geisler, C., Robbe, D., Zugaro, M., Sirota, A., and Buzsáki, G. (2007). Hippocampal place cell assemblies are speed-controlled oscillators. *Proc. Natl. Acad. Sci. USA* 104, 8149–8154.
52. McClain, K., Tingley, D., Heeger, D.J., and Buzsáki, G. (2019). Position-theta-phase model of hippocampal place cell activity applied to quantification of running speed modulation of firing rate. *Proc. Natl. Acad. Sci. USA* 116, 27035–27042.
53. Muller, R.U., Kubie, J.L., and Ranck, J.B., Jr. (1987). Spatial firing patterns of hippocampal complex-spike cells in a fixed environment. *J. Neurosci.* 7, 1935–1950.
54. Muller, R.U., Bostock, E., Taube, J.S., and Kubie, J.L. (1994). On the directional firing properties of hippocampal place cells. *J. Neurosci.* 14, 7235–7251.
55. Knierim, J.J., Kudrimoti, H.S., and McNaughton, B.L. (1995). Place cells, head direction cells, and the learning of landmark stability. *J. Neurosci.* 15, 1648–1659.
56. Samsonovich, A., and McNaughton, B.L. (1997). Path integration and cognitive mapping in a continuous attractor neural network model. *J. Neurosci.* 17, 5900–5920.
57. Jeffery, K.J., and O'Keefe, J.M. (1999). Learned interaction of visual and idiothetic cues in the control of place field orientation. *Exp. Brain Res.* 127, 151–161.
58. Chakraborty, S., Anderson, M.I., Chaudhry, A.M., Mumford, J.C., and Jeffery, K.J. (2004). Context-independent directional cue learning by hippocampal place cells. *Eur. J. Neurosci.* 20, 281–292.
59. Aikath, D., Weible, A.P., Rowland, D.C., and Kentros, C.G. (2014). Role of self-generated odor cues in contextual representation. *Hippocampus* 24, 1039–1051.
60. Calton, J.L., Stackman, R.W., Goodridge, J.P., Archey, W.B., Dudchenko, P.A., and Taube, J.S. (2003). Hippocampal place cell instability after lesions of the head direction cell network. *J. Neurosci.* 23, 9719–9731.
61. Harvey, R.E., Rutan, S.A., Willey, G.R., Siegel, J.J., Clark, B.J., and Yoder, R.M. (2018). Linear self-motion cues support the spatial distribution and stability of hippocampal place cells. *Curr. Biol.* 28, 1803–1810.e5.
62. Muller, R.U., and Kubie, J.L. (1987). The effects of changes in the environment on the spatial firing of hippocampal complex-spike cells. *J. Neurosci.* 7, 1951–1968.
63. Scaplen, K.M., Gulati, A.A., Heimer-McGinn, V.L., and Burwell, R.D. (2014). Objects and landmarks: hippocampal place cells respond differently to manipulations of visual cues depending on size, perspective, and experience. *Hippocampus* 24, 1287–1299.

Current Biology

Article



64. Sharp, P.E., Blair, H.T., Etkin, D., and Tzanatos, D.B. (1995). Influences of vestibular and visual motion information on the spatial firing patterns of hippocampal place cells. *J. Neurosci.* 15, 173–189.
65. Zittrell, F. (2019). CircHist: circular histogram in MATLAB. Zenodo. <https://zenodo.org/record/3445084#.Xv6g1Od7IPY>.
66. Huxter, J., Burgess, N., and O'Keefe, J. (2003). Independent rate and temporal coding in hippocampal pyramidal cells. *Nature* 425, 828–832.
67. Climer, J.R., DiTullio, R., Newman, E.L., Hasselmo, M.E., and Eden, U.T. (2015). Examination of rhythmicity of extracellularly recorded neurons in the entorhinal cortex. *Hippocampus* 25, 460–473.
68. Hinman, J.R., Brandon, M.P., Climer, J.R., Chapman, G.W., and Hasselmo, M.E. (2016). Multiple running speed signals in medial entorhinal cortex. *Neuron* 91, 666–679.
69. Jeewajee, A., Barry, C., O'Keefe, J., and Burgess, N. (2008). Grid cells and theta as oscillatory interference: electrophysiological data from freely-moving rats. *Hippocampus* 18, 1175–1185.
70. Maurer, A.P., Vanrhoads, S.R., Sutherland, G.R., Lipa, P., and McNaughton, B.L. (2005). Self-motion and the origin of differential spatial scaling along the septo-temporal axis of the hippocampus. *Hippocampus* 15, 841–852.
71. Welday, A.C., Shlifer, I.G., Bloom, M.L., Zhang, K., and Blair, H.T. (2011). Cosine directional tuning of theta cell burst frequencies: evidence for spatial coding by oscillatory interference. *J. Neurosci.* 31, 16157–16176.
72. Stensola, H., Stensola, T., Solstad, T., Frøland, K., Moser, M.-B., and Moser, E.I. (2012). The entorhinal grid map is discretized. *Nature* 492, 72–78.
73. Petersen, P.C., and Buzsáki, G. (2020). Cooling of medial septum reveals theta phase lag coordination of hippocampal cell assemblies. *Neuron*. Published online June 10, 2020. <https://doi.org/10.1016/j.neuron.2020.05.023>.
74. Góis, Z.H.T.D., and Tort, A.B.L. (2018). Characterizing speed cells in the rat hippocampus. *Cell Rep.* 25, 1872–1884.e4.
75. Wiener, S.I., Paul, C.A., and Eichenbaum, H. (1989). Spatial and behavioral correlates of hippocampal neuronal activity. *J. Neurosci.* 9, 2737–2763.
76. O'Keefe, J., Burgess, N., Donnett, J.G., Jeffery, K.J., and Maguire, E.A. (1998). Place cells, navigational accuracy, and the human hippocampus. *Philos. Trans. R. Soc. Lond. B Biol. Sci.* 353, 1333–1340.
77. Zhang, K., Ginzburg, I., McNaughton, B.L., and Sejnowski, T.J. (1998). Interpreting neuronal population activity by reconstruction: unified framework with application to hippocampal place cells. *J. Neurophysiol.* 79, 1017–1044.
78. Czurkó, A., Hirase, H., Csicsvari, J., and Buzsáki, G. (1999). Sustained activation of hippocampal pyramidal cells by 'space clamping' in a running wheel. *Eur. J. Neurosci.* 11, 344–352.
79. Hirase, H., Czurkó, A., Csicsvari, J., and Buzsáki, G. (1999). Firing rate and theta-phase coding by hippocampal pyramidal neurons during 'space clamping'. *Eur. J. Neurosci.* 11, 4373–4380.
80. Ekstrom, A.D., Meltzer, J., McNaughton, B.L., and Barnes, C.A. (2001). NMDA receptor antagonism blocks experience-dependent expansion of hippocampal "place fields". *Neuron* 31, 631–638.
81. Nitz, D., and McNaughton, B. (2004). Differential modulation of CA1 and dentate gyrus interneurons during exploration of novel environments. *J. Neurophysiol.* 91, 863–872.
82. Kropff, E., Carmichael, J.E., Moser, M.-B., and Moser, E.I. (2015). Speed cells in the medial entorhinal cortex. *Nature* 523, 419–424.
83. Fontaine, C.J., Patten, A.R., Sickmann, H.M., Helper, J.L., and Christie, B.R. (2016). Effects of pre-natal alcohol exposure on hippocampal synaptic plasticity: sex, age and methodological considerations. *Neurosci. Biobehav. Rev.* 64, 12–34.
84. Savage, D.D., Rosenberg, M.J., Wolff, C.R., Akers, K.G., El-Emawy, A., Staples, M.C., Varaschin, R.K., Wright, C.A., Seidel, J.L., Caldwell, K.K., and Hamilton, D.A. (2010). Effects of a novel cognition-enhancing agent on fetal ethanol-induced learning deficits. *Alcohol. Clin. Exp. Res.* 34, 1793–1802.
85. Galindo, R., Frausto, S., Wolff, C., Caldwell, K.K., Perrone-Bizzozero, N.I., and Savage, D.D. (2004). Prenatal ethanol exposure reduces mGluR5 receptor number and function in the dentate gyrus of adult offspring. *Alcohol. Clin. Exp. Res.* 28, 1587–1597.
86. Varaschin, R.K., Allen, N.A., Rosenberg, M.J., Valenzuela, C.F., and Savage, D.D. (2018). Prenatal alcohol exposure increases histamine H₃ receptor-mediated inhibition of glutamatergic neurotransmission in rat dentate gyrus. *Alcohol. Clin. Exp. Res.* 42, 295–305.
87. Latuske, P., Kornienko, O., Kohler, L., and Allen, K. (2018). Hippocampal remapping and its entorhinal origin. *Front. Behav. Neurosci.* 11, 253.
88. Hales, J.B., Schlesiger, M.I., Leutgeb, J.K., Squire, L.R., Leutgeb, S., and Clark, R.E. (2014). Medial entorhinal cortex lesions only partially disrupt hippocampal place cells and hippocampus-dependent place memory. *Cell Rep.* 9, 893–901.
89. Schlesiger, M.I., Boublik, B.L., Hales, J.B., Leutgeb, J.K., and Leutgeb, S. (2018). Hippocampal global remapping can occur without input from the medial entorhinal cortex. *Cell Rep.* 22, 3152–3159.
90. Van Cauter, T., Poucet, B., and Save, E. (2008). Unstable CA1 place cell representation in rats with entorhinal cortex lesions. *Eur. J. Neurosci.* 27, 1933–1946.
91. Brun, V.H., Leutgeb, S., Wu, H.Q., Schwarzs, R., Witter, M.P., Moser, E.I., and Moser, M.B. (2008). Impaired spatial representation in CA1 after lesion of direct input from entorhinal cortex. *Neuron* 57, 290–302.
92. Terrazas, A., Krause, M., Lipa, P., Gothard, K.M., Barnes, C.A., and McNaughton, B.L. (2005). Self-motion and the hippocampal spatial metric. *J. Neurosci.* 25, 8085–8096.
93. Yoganarasimha, D., Yu, X., and Knierim, J.J. (2006). Head direction cell representations maintain internal coherence during conflicting proximal and distal cue rotations: comparison with hippocampal place cells. *J. Neurosci.* 26, 622–631.
94. McNaughton, B.L., Battaglia, F.P., Jensen, O., Moser, E.I., and Moser, M.B. (2006). Path integration and the neural basis of the 'cognitive map'. *Nat. Rev. Neurosci.* 7, 663–678.
95. Yoder, R.M., Clark, B.J., and Taube, J.S. (2011). Origins of landmark encoding in the brain. *Trends Neurosci.* 34, 561–571.
96. Neunuebel, J.P., Yoganarasimha, D., Rao, G., and Knierim, J.J. (2013). Conflicts between local and global spatial frameworks dissociate neural representations of the lateral and medial entorhinal cortex. *J. Neurosci.* 33, 9246–9258.
97. Cacucci, F., Yi, M., Wills, T.J., Chapman, P., and O'Keefe, J. (2008). Place cell firing correlates with memory deficits and amyloid plaque burden in Tg2576 Alzheimer mouse model. *Proc. Natl. Acad. Sci. USA* 105, 7863–7868.
98. Lester, A.W., Moffat, S.D., Wiener, J.M., Barnes, C.A., and Wolbers, T. (2017). The aging navigational system. *Neuron* 95, 1019–1035.
99. Hamilton, D.A., Kodituwakk, P., Sutherland, R.J., and Savage, D.D. (2003). Children with fetal alcohol syndrome are impaired at place learning but not cued-navigation in a virtual Morris water task. *Behav. Brain Res.* 143, 85–94.
100. Knierim, J.J., and Hamilton, D.A. (2011). Framing spatial cognition: neural representations of proximal and distal frames of reference and their roles in navigation. *Physiol. Rev.* 91, 1245–1279.
101. Winson, J. (1978). Loss of hippocampal theta rhythm results in spatial memory deficit in the rat. *Science* 201, 160–163.
102. Lenck-Santini, P.P., and Holmes, G.L. (2008). Altered phase precession and compression of temporal sequences by place cells in epileptic rats. *J. Neurosci.* 28, 5053–5062.
103. Robbe, D., and Buzsáki, G. (2009). Alteration of theta timescale dynamics of hippocampal place cells by a cannabinoid is associated with memory impairment. *J. Neurosci.* 29, 12597–12605.

104. Kim, J., Delcasso, S., and Lee, I. (2011). Neural correlates of object-in-place learning in hippocampus and prefrontal cortex. *J. Neurosci.* 31, 16991–17006.
105. Madden, J.T., Thompson, S.M., Magcalas, C.M., Wagner, J.L., Hamilton, D.A., Savage, D.D., Clark, B.J., and Pentkowski, N.S. (2020). Moderate prenatal alcohol exposure reduces parvalbumin expressing GABAergic interneurons in the dorsal hippocampus of adult male and female rat offspring. *Neurosci. Lett.* 718, 134700.
106. Amilhon, B., Huh, C.Y., Manseau, F., Ducharme, G., Nichol, H., Adamantidis, A., and Williams, S. (2015). Parvalbumin interneurons of hippocampus tune population activity at theta frequency. *Neuron* 86, 1277–1289.
107. Hu, H., Gan, J., and Jonas, P. (2014). Interneurons. Fast-spiking, parvalbumin⁺ GABAergic interneurons: from cellular design to microcircuit function. *Science* 345, 1255263.
108. Royer, S., Zemelman, B.V., Losonczy, A., Kim, J., Chance, F., Magee, J.C., and Buzsáki, G. (2012). Control of timing, rate and bursts of hippocampal place cells by dendritic and somatic inhibition. *Nat. Neurosci.* 15, 769–775.
109. Climer, J.R., Newman, E.L., and Hasselmo, M.E. (2013). Phase coding by grid cells in unconstrained environments: two-dimensional phase precession. *Eur. J. Neurosci.* 38, 2526–2541.
110. Berens, P. (2009). CircStat: a MATLAB toolbox for circular statistics. *J. Stat. Softw.* 31, 1–21.
111. Ahmed, O.J., and Mehta, M.R. (2009). The hippocampal rate code: anatomy, physiology and theory. *Trends Neurosci.* 32, 329–338.
112. Butler, W.N., Hardcastle, K., and Giocomo, L.M. (2019). Remembered reward locations restructure entorhinal spatial maps. *Science* 363, 1447–1452.
113. Ravassard, P., Kees, A., Willers, B., Ho, D., Aharoni, D.A., Cushman, J., Aghajan, Z.M., and Mehta, M.R. (2013). Multisensory control of hippocampal spatiotemporal selectivity. *Science* 340, 1342–1346.
114. Jammalamadaka, S.R., and Sengupta, A. (2001). *Topics in Circular Statistics* (World Scientific).
115. Kempter, R., Leibold, C., Buzsáki, G., Diba, K., and Schmidt, R. (2012). Quantifying circular-linear associations: hippocampal phase precession. *J. Neurosci. Methods* 207, 113–124.
116. Skaggs, W.E., McNaughton, B.L., Wilson, M.A., and Barnes, C.A. (1996). Theta phase precession in hippocampal neuronal populations and the compression of temporal sequences. *Hippocampus* 6, 149–172.
117. Burgess, N., Recce, M., and O'Keefe, J. (1994). A model of hippocampal function. *Neural Netw.* 7, 1065–1081.
118. Harris, K.D., Henze, D.A., Hirase, H., Leinekugel, X., Dragoi, G., Czurkó, A., and Buzsáki, G. (2002). Spike train dynamics predicts theta-related phase precession in hippocampal pyramidal cells. *Nature* 417, 738–741.
119. Huxter, J.R., Senior, T.J., Allen, K., and Csicsvari, J. (2008). Theta phase-specific codes for two-dimensional position, trajectory and heading in the hippocampus. *Nat. Neurosci.* 11, 587–594.
120. Jeewajee, A., Barry, C., Douchamps, V., Manson, D., Lever, C., and Burgess, N. (2013). Theta phase precession of grid and place cell firing in open environments. *Philos. Trans. R. Soc. Lond. B Biol. Sci.* 369, 20120532.
121. Munn, R.G.K., Mallory, C.S., Hardcastle, K., Chetkovich, D.M., and Giocomo, L.M. (2020). Entorhinal velocity signals reflect environmental geometry. *Nat. Neurosci.* 23, 239–251.
122. Cooper, H., and Hedges, L.V. (1993). *The Handbook of Research Synthesis* (Russell Sage Foundation).

STAR★METHODS

KEY RESOURCES TABLE

REAGENT or RESOURCE	SOURCE	IDENTIFIER
Deposited Data		
Datasets	This paper	https://doi.org/10.17605/OSF.IO/PM89Y
Experimental Models: Organisms/Strains		
Rat: Long-Evans	Harlan Industries	
Software and Algorithms		
Data Acquisition Software	Cheetah (Neuralynx)	https://neuralynx.com
Analysis Software	MATLAB v2017, 2018, 2019	https://www.mathworks.com/
Analysis Software	RStudio	https://rstudio.com/
Custom Code for Data Analysis	This paper	https://github.com/ryanharvey1/ephys_tools
Pass Index	[109]	https://github.com/jrclimer/Pass_Index
Theta-rhythmicity	[67]	https://github.com/jrclimer/mle_rhythmicity
Circular Statistics Toolbox	[110]	https://www.mathworks.com/matlabcentral/fileexchange/10676-circular-statistics-toolbox-directional-statistics
Spike Sorting	Klustakwik	http://klustakwik.sourceforge.net/
Spike Sorting	Kilosort2	https://github.com/MouseLand/Kilosort2
Spike sorting	MClust	https://github.com/adredish/MClust-Spike-Sorting-Toolbox
Spike sorting	Phy	https://github.com/cortex-lab/phy
Other		
Custom electrodes (8 tetrodes)	Custom built	
Halo-18 Microdrive (16 tetrodes)	Neuralynx	https://neuralynx.com/hardware/halo-18-microdrive
Digital Neuralynx recording system, Lynx SX	Neuralynx	https://neuralynx.com
17um dia nichrome wire	California fine wire	https://www.calfinewire.com/index.html

RESOURCE AVAILABILITY

Lead Contact

Further information, materials, and protocols used in the manuscript will be made available upon request to the Lead Contact author, Benjamin J. Clark (e-mail: bnjclark@unm.edu).

Materials Availability

This study did not generate new unique reagents.

Data and Code Availability

The datasets generated during this study are available at OSF: <https://doi.org/10.17605/OSF.IO/PM89Y>. Custom code is available at https://github.com/ryanharvey1/ephys_tools

EXPERIMENTAL MODEL AND SUBJECT DETAILS

Subjects

Subjects were 17 male Long-Evans rats obtained from the University of New Mexico Health Sciences Center Animal Resource Facility (see breeding protocol below). After weaning, all animals were pair-housed in standard plastic cages with water and food available *ad libitum*. All cage-mate pairs were matched for age and weight and animals were at least 4 months of age before testing. Saccharin-exposed control ($n = 9$) and prenatal-alcohol-exposed (PAE) ($n = 8$) rats began linear track and cylinder behavioral training at 46 months of age. At this time, rats weights were slowly brought down to approximately 90 percent of their *ad libitum* weight. Lights were maintained on a reverse 12 h:12 h light:dark cycle with lights on at 0900 h. All procedures were approved by the Institutional Animal Care and Use Committee of either the main campus or Health Sciences Center at the University of New Mexico.

Breeding and voluntary ethanol consumption

Breeding procedures were conducted at the University of New Mexico Health Sciences Animal Resource Facility. Three to four-month-old female breeders (Harlan Industries, Indianapolis, IN) were single housed in standard plastic cages and placed on a 12-hour reverse light: dark cycle (lights on from 2100–0900 h) and kept at 22 °C with *ad libitum* food and water. Following a one-week acclimation period in the animal facility, the breeders were exposed to a voluntary ethanol drinking paradigm (Figure 1A). Female rats were provided 0.066% (w/v) saccharin in tap water from 1000–1400 h (4 h) each day. On days 12, the saccharin water contained 0% ethanol, on days 34 saccharin water contained 2.5% ethanol (v/v), and on day 5 and thereafter, saccharin water contained 5% ethanol (v/v). The daily four-hour consumption of ethanol was monitored for at least two weeks and the mean daily ethanol consumption was determined for each female. After two weeks of daily ethanol consumption, females that drank at levels less than one standard deviation below that of the entire group mean were removed from the study (~1215% of all female rats). The remaining females were then assigned to either a saccharin control or 5% ethanol drinking group. These breeding females were matched such that the mean pre-pregnancy ethanol consumption by each group was similar. As a result, the dams of both groups experience equivalent pre-conceptual exposure to ethanol. Lastly, the female breeders were nulliparous and were not used in multiple rounds of breeding, while the male rats were experienced breeders.

Female rats were matched with a male breeder rat until pregnancy was verified, based on the presence of a vaginal plug. There was no ethanol consumption during breeding. Beginning on gestational day 1, the rat dams were given access to saccharin (Sigma Life Sciences, St. Louis, Missouri) water containing either 0% (v/v) or 5% (v/v) ethanol (Koptec, King of Prussia, Pennsylvania) for four hours a day, from 1000–1400 h. The volume of the 0% ethanol saccharin water provided to the control group was matched to the mean volume of the 5% ethanol saccharin water consumed by the ethanol group. During gestation and including the four-hour ethanol/saccharin drinking period, rats were provided with *ad libitum* water and rat chow (Teklad global soy protein-free extruded food 2920). Daily ethanol consumption was recorded for each rat dam (Table S1). The daily mean ethanol consumption throughout pregnancy was 1.96 ± 0.14 g/kg and did not vary significantly during each of the three weeks of gestation. In a separate set of rat dams, this level of ethanol consumption has been shown to produce a mean peak maternal serum ethanol concentration of 60.8 ± 5.8 mg/dl [44]. Daily ethanol consumption ended at birth, and the litters were weighed and culled to 10 pups. As shown in Table S1, this moderate exposure paradigm did not affect maternal weight gain, offspring litter size, or birth weight for the offspring used in these studies. Experimental offspring used in these studies were generated from nine different saccharin control and eight different ethanol-consuming rat dams bred in four separate breeding rounds.

METHOD DETAILS

Surgical procedures

Rats were anesthetized with isoflurane and positioned in a stereotaxic apparatus (David Kopf Instruments) with bregma and lambda set at the same D-V plane. The scalp was retracted, and a hole was drilled above the hippocampus. Six additional holes were drilled in the frontal, parietal, and occipital bones to hold jewelers screws with a single screw in the parietal plate used for grounding. With the electrode bundle (see below for fabrication details) positioned dorsal to the hippocampus (Figure 1A), the drive assemblies were fastened to the skull and jewelers screws with dental acrylic. The scalp was sutured around the electrode drive and the wound was covered with Neosporin. Buprenorphine was administered postoperatively and the animal was allowed to recover at least 1 week before recording.

Apparatus

The cylinder (diameter: 76.5 cm, height: 40 cm) was positioned on a black plastic surface, and a white cue card covered 100 degrees of the wall surface (Figure 1B). The linear track (length: 120 cm, width: 9 cm, height: 10 cm) was positioned relative to polarizing distal cues (white cue cards) to make each running direction distinct. The entire recording area was located within a large Faraday cage to reduce electrical noise. Eight battery-powered LED lights mounted on the ceiling provided illumination.

Behavioral training

Each animal was exposed to each maze for several days. On the linear track, animals were trained to continuously alternate between the two ends. Stop locations were rewarded with 1/8 piece of a fruit-loop if animals completed a successful lap without stopping or alternating the incorrect direction. This training continued until 40 laps could be completed within 15 minutes. For the cylinder, animals were trained to randomly forage for fruit-loop pieces that were semi-randomly dropped into the environment until all locations were sufficiently sampled. Experimenters were aware of each animals group affiliation (PAE or control) upon initiation of behavioral training.

Recording Procedures

Single units and local field potentials (LFP) were recorded from the CA1 and CA3 regions of the dorsal hippocampus using 8 to 16 tetrodes each of which consisting of four-channel electrodes constructed by twisting together strands of insulated 12–17 µm nichrome wire [17].

After surgery, tetrodes were slowly advanced into the CA1 area of the hippocampus. During tetrode advancement and recordings, the electrode assembly was connected to a multichannel, impedance matching, unity gain preamplifier headstage. The output was

routed to a data acquisition system with 64 digitally programmable differential amplifiers (Neuralynx, Bozeman, MT, USA). Spike waveforms above a threshold of 30–40 µV were time-stamped, digitized at 32 kHz, and later imported into MClust for spike sorting. Continuous wide-band signals from each channel were collected for sessions spike sorted with kilosort2. The rats position was tracked and sampled at 30 Hz by recording the position of light-emitting diodes that were placed above the head.

Rats were screened each day on a pedestal for identifiable units and HPC theta rhythm visible in the local field potentials. Once units and theta rhythm were found a typical recording began with ~40 laps on a linear track (~10–15 minutes), followed by an open field cylinder session, and finished with an open field cylinder session with the local cue rotated 90 degrees (Figure 1B). Linear track sessions in which the rat made less than 15 laps were not included in any analysis. In the cylinder sessions, rats randomly foraged for fruit-loops until the environment was fully sampled (~15–30 minutes). Depending on the rats motivation, some sessions were limited to either a single linear track or a linear track and one cylinder session. After each daily recording session, tetrodes were advanced approximately 62 µm to record different neurons each day. Each rat performed 32 daily sessions on average.

Histology

Rats were euthanized by transcardial perfusion with normal saline followed by 10% Formalin, and brains were then placed in Formalin for 24 hours to ensure adequate fixation. Brains were then placed in 20% sucrose for cryoprotection before they were sectioned at 40 µm on a freezing microtome. Brain sections were mounted on gelatin-coated or charged microscope slides and stained with Cresyl violet (Figure 1A). The electrode position at the time of each recording was estimated relative to the site of the final electrode tip location. Electrode tips were marked by applying constant current (4 mA for 4 s) through a wire of each tetrode. Our analyses included only sessions where the electrode tip was estimated to be located within CA1 and CA3 regions. It is important to note the possibility that a small number of recordings may have included granule cells or mossy cells from the dentate subregion, given its proximity to CA3.

Spike sorting

Spike sorting was performed first by using unsupervised methods klustakwik (<http://klustakwik.sourceforge.net/>) or kilosort2 (<https://github.com/MouseLand/Kilosort2>) with manual refinement conducted in MClust (<https://github.com/adredish/MClust-Spike-Sorting-Toolbox>) or Phy (<https://github.com/cortex-lab/phy>). Autocorrelation and cross-correlation functions were used as single unit identification criteria for both methods. Active neurons, defined as having at least 100 spikes and a peak firing rate of 1Hz, were considered for analysis.

Spatial rate map construction

First, position and spiking data were speed filtered; only epochs with instantaneous running speeds of 3 cm/sec or more were included. Then occupancy normalized firing rate maps were constructed using 3x3cm spatial bins. Maps were then smoothed with a 5x5 standard deviation Gaussian kernel. For linear track tuning curves, the x coordinate was binned as above while the y-coordinate was compressed into a single bin.

Spatial information

Spatial information content for each cell, the spatial information content was calculated as:

$$\text{Information} = \sum_{i=1}^N P_i \frac{\lambda_i}{\lambda} \log_2 \frac{\lambda_i}{\lambda} \quad (\text{Equation 1})$$

Where the environment is divided into spatial bins $i = 1, \dots, N$, P_i is the occupancy probability of bin i , λ_i is the mean firing rate for bin i , and λ is the overall mean firing rate of the cell [111]

Sparsity

Sparsity for each cell was calculated as:

$$\text{Sparsity} = \frac{\left(\frac{1}{n} \sum_i r_i\right)^2}{\frac{1}{n} \sum_i (r_i^2)} \quad (\text{Equation 2})$$

Where i is a spatial bin and r_i is the firing rate of the cell in bin i of an environment containing a total of n spatial bins [111]. A sparsity value of 1 implies no sparseness. A sparsity value approaching 0 is indicative of maximal sparseness and implies a greater amount of spatial information in each spike emitted by that cell.

Spatial correlation

The spatial similarity of place fields across two conditions was calculated using Pearson's correlation. The correlation coefficient was calculated by comparing the firing rates between all pixels at corresponding locations.

$$r = \frac{\sum_m \sum_n (A_{mn} - \bar{A})(B_{mn} - \bar{B})}{\sqrt{\left(\sum_m \sum_n (A_{mn} - \bar{A})^2\right) \left(\sum_m \sum_n (B_{mn} - \bar{B})^2\right)}} \quad (\text{Equation 3})$$

Spatial coherence

Spatial coherence was computed as the Fisher z-transformation (the arctangent) of the correlation between the firing rate of each spatial bin and the average firing rate of the neighboring 3-8 spatial bins [112].

Directionality Index

The directionality of a cell on the linear track was defined as:

$$D = \frac{\left| \sum_i (\lambda_{iF} - \lambda_{iB}) \right|}{\sum_i (\lambda_{iF} + \lambda_{iB})} \quad (4)$$

Where λ_{iF} is the firing rate in bin i in the forward (or outbound) running direction and λ_{iB} is the firing rate in the backward (or inbound) running direction [113]. This equation was also used to compare rate differences between the two cylinder sessions.

Place cell classification

From neurons recorded during the linear track sessions, the set of heuristics used to identify a place field were the following 1) Minimum peak firing rate of 1 Hz, 2) Minimum field width of 9 cm, 3) Maximum field width of 78 cm (65% of track length), 4) At least 15 laps with consistent behavior, 5) At least 100 spikes, 6) Minimum spatial information content of 0.15 bits/spike. Given these criteria, 24.6% (1459 of 5927) of active (> 100 spikes & > 1 Hz peak rate) HPC neurons had at least one place field with a mean of 1.26 ± 0.01 per neuron. No limit was set on the number of place fields single neurons could have and metrics were obtained from the field with the highest firing rate. The median peak firing rate was 7.52 ± 0.32 Hz, and the mean field width was 45.93 ± 0.40 cm. The start and stop position for each field were taken as the spatial bins where the firing rate drops below 20% of the peak firing rate. From neurons recorded in the cylinder sessions, a similar set of heuristics used to identify a place field were the following 1) Minimum peak firing rate of 1 Hz, 2) Minimum field width of 9 cm, 3) Maximum field width of 49.7 cm (65% of cylinder diameter), 4) At least 100 spikes, 5) Minimum spatial information content of 0.15 bits/spike. Given these criteria, 24.1% (1554 of 6448) of HPC active neurons recorded during the first cylinder session had at least one place field with a mean of 1.74 ± 0.02 fields per neuron. While there were no limits set on the number of place fields single neurons could have, place cell metrics were obtained from the field with the highest firing rate. The median peak firing rate was 7.25 ± 0.33 Hz, and the mean field width was 31.71 ± 0.25 cm. The field boundaries were drawn using Matlab's contour function following a k-means clustering procedure which separated low and high firing locations.

Cue rotation analysis

A rotational correlation analysis was used to assess the response of place cells following the 90-degree cue rotation by first rotating the rate map from the cue rotation session in 6-degree bins while calculating a spatial correlation for each rotation. Next, the angle at which the two rate maps showed the highest correlation was declared the cell's rotation angle. Consistent with previous literature, cells below a moderate correlation, $r < 0.4$, were not used in this analysis in an attempt to minimize the impact of spontaneous remapping which would result in erroneous rotation angles [55, 59–64]. A depiction of this analysis can be found in Figure 4A.

Instantaneous theta phase, firing phase

A 3rd order Butterworth band-pass filter (412Hz) was applied to the LFP signal from a single channel on each tetrode selected for phase estimation. The instantaneous theta phase was obtained from the Hilbert transform of the filtered signal. Spike and LFP time-stamps were then used to linearly interpolate the firing phase from these values.

Theta phase precession

One-dimensional phase precession of place cells in the linear track was quantified using a circular-linear correlation between theta firing phase from each place cell and the linear x coordinate as the rat passed through a place field [114, 115]. Phase precession was quantified for multiple place fields from a single cell. However, metrics for comparison were only taken from the place field with the highest peak firing rate.

While theta phase precession was initially discovered as in rats while they ran back and forth along a linear track [17], the phenomenon also occurs in open spaces [109, 116, 117–120]. Two-dimensional phase precession of place cells in the cylinder was computed using 'pass-index' https://github.com/jrclimer/Pass_Index [109]. Rate maps were smoothed with a pseudo-Gaussian kernel with a five-bin standard deviation. The value at each bin was then percentile normalized between 0 and 1 which resulted in the field index map. The trajectory of the animal was sampled evenly along the arc-length of the trajectory at as many points as there were position tracking samples (30 Hz). The nearest bins were then found by minimizing the difference between the x and y positions and the center of the bins via the MATLAB function: bsxfun. The omnidirectional pass index was then computed on the field index

maps which resulted in a -1 to 1 vector where -1 represents when the animal was at the beginning of the place field, 0 represents the center, and $+1$ represents the end of the place field. A circular-linear correlation between theta firing phase from each cell and the above vector to quantification of phase precession [114, 115].

Spike-train theta rhythmicity

We assessed the properties of theta-rhythmicity, such as intrinsic theta-frequency, rhythmicity magnitude, and approximated best fit autocorrelograms, and running speed covariation using a maximum likelihood estimation approach [67, 68] (available at https://github.com/jrclimer/mle_rhythmicity).

Speed modulated cells

Analysis of speed modulation of firing rates was similar to previous approaches [82, 121] was adapted from code located at https://github.com/GiocomoLab/Munn_et_al_2019. Speed scores were calculated as the Pearson correlation between the instantaneous firing rate of each cell and the running speed of the animal across 200ms time bins. As well, overall slopes and intercepts were determined for each cell by the fitting of first-degree (linear) polynomials using the polyfit function in MATLAB. To determine if a cell was speed modulated, either positively or negatively, a null distribution was created for each cell by shuffling the spike train 100 times in a random interval 20 s before to 20 s after its true position and calculating a speed score each iteration. Cells were considered speed modulated if the proportion of permutations with a larger magnitude was < 0.05 .

Speed by firing rate tuning curves, shown in Figure S5, were generated by averaging instantaneous firing rates over 2cm/sec speed bins ranging from 0cm/sec to the 95th percentile of the animal's running speed for that particular session.

QUANTIFICATION AND STATISTICAL ANALYSIS

Data analysis

Data analysis was performed by importing position data, LFP data, and spike data into MATLAB and further processing the data with custom-written software. Statistical analysis was performed in MATLAB and R.

Statistical Analysis

All statistical tests used were two-sided, and the significance threshold for all tests was set at $p < 0.05$ unless otherwise stated. All main tests are shown in Table S2.

The normality of distributions was not assumed, so comparisons were made using non-parametric statistics. For between-group comparison, Wilcoxon signed-rank or Wilcoxon rank-sum tests were used to test the equality of medians. Effect sizes (r) for Wilcoxon tests were calculated with $r = Z / \sqrt{n}$ [122]. Group comparisons of continuous data were visualized using violin plots to show the distribution density and overlaid boxplots to show the median, interquartile range (IQR), and 1.5 times the IQR. IQR = quartile 3 – quartile 1 and is represented by the box length. The uppermost line is quartile 3 + 1.5 IQR, whereas the lowermost line is quartile 1 – 1.5 IQR. Between-group comparison of proportions were computed using chi-square tests and visualized with bar plots. Effect sizes for these comparisons were calculated with Cramér's V.

Angular data were assessed using the Circular Statistics Toolbox [110]. Verification of von mises distributions were performed using Rayleigh Tests, while a Watson-Williams multi-sample test for equal means was used to compare mean directions between groups.

Current Biology, Volume 30

Supplemental Information

**Altered Hippocampal Place Cell
Representation and Theta Rhythmicity
following Moderate Prenatal Alcohol Exposure**

Ryan E. Harvey, Laura E. Berkowitz, Daniel D. Savage, Derek A. Hamilton, and Benjamin J. Clark

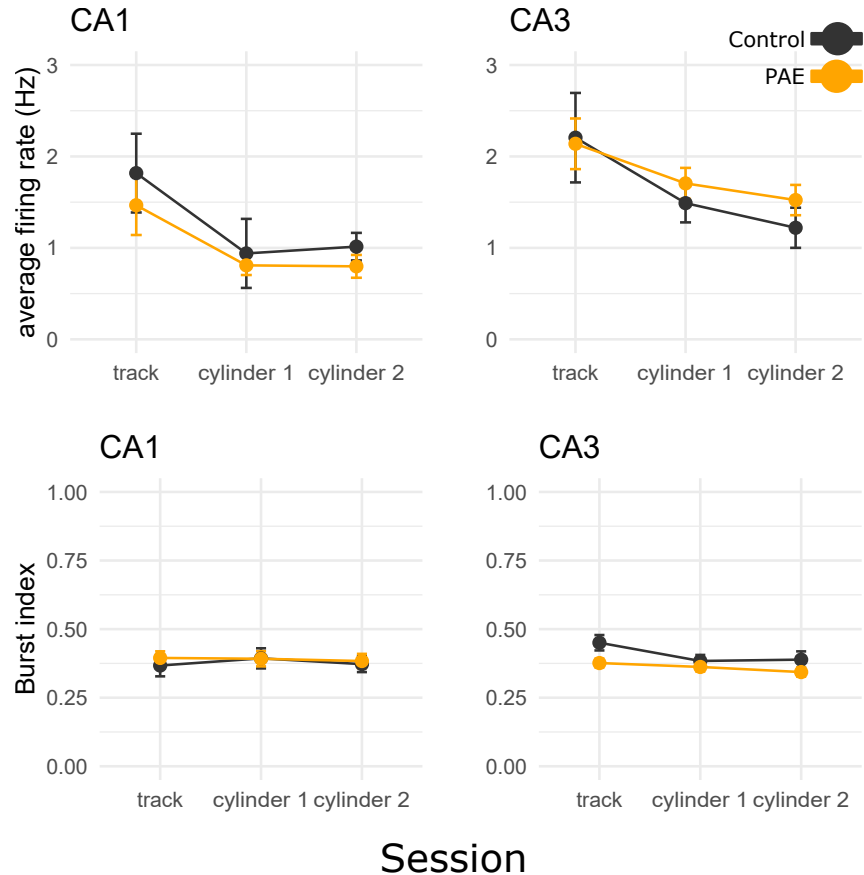


Figure S1: Average firing rate and burst index over recording sessions. Related to Figure 1. While CA1 average firing rates were similar between groups across sessions (all $p \geq 0.03174$, WRS), CA1 and CA3 cells from both groups displayed decreased average firing rates in the first and second cylinder session compared to the linear track (control: $p < 0.0005$, PAE: $p < 0.0001$; Paired WRS), but had similar rates between cylinder sessions (control: $p \geq 0.0303$, PAE: $p \geq 0.4357$, Paired WRS). Burst index was calculated as the difference between the cell's burst rate and the expected burst rate derived from a homogeneous Poisson process with the same average firing rate. Bursts were defined as epochs of spikes with interspike intervals between 0ms and 10ms. Burst index from CA1 and CA3 cells was similar between groups across sessions (all $p \geq 0.01567$, WRS). However, control CA3 cells displayed a decrease in burst index from the linear track to the first and second cylinder sessions (all $p \leq 0.0009$, Paired WRS). Data is represented as median \pm standard error of the median. Neurons included met place cell criteria in each maze. Family-wise error was maintained at $\alpha \leq 0.05$ by adjusting the significance levels for individual tests to $\alpha \leq 0.005$.

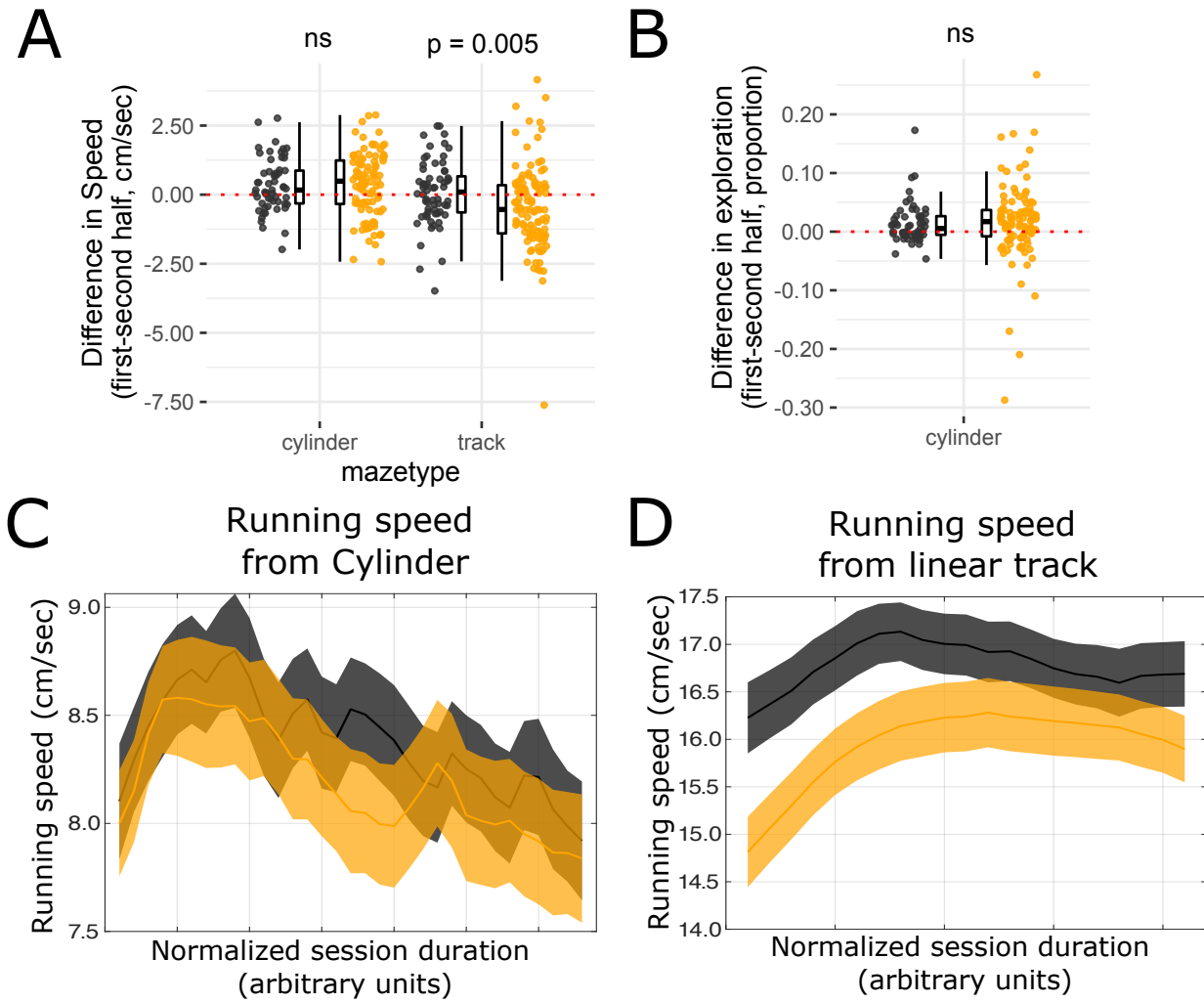


Figure S2: Behavioral stability between the first and second half of the session. Related to Figure 2. (A) Difference in running speed between the first and second halves of each recording session. PAE rats have a larger difference in running speed on the linear between the two halves compared to control rats ($p = 0.005$, WRS, effect size (r) = 0.21, Control median = 0.09, $n = 64$; PAE median = -0.54, $n = 111$). (B) Difference in the proportion of the cylinder explored between the first and second halves of each recording session was similar between groups. Note that both medians are above 0 indicating that exploration was higher in the first half compared to the second half of the session. Linear track data is not shown here because the extent of the track was sampled with each lap and rats from both groups completed similar numbers of laps. (C-D) Running speed over the duration of the cylinder sessions. (D) Running speed over the duration of the linear track sessions. Note the group difference here reflects the significant difference in A where PAE rats have a slightly slower running speed at the start of the trial. (C-D) Because all recording sessions had slightly different recording durations depending on the rat's motivation, we first calculated mean velocity from each session over 1 minute bins. The resulting speed vectors were linearly interpolated as to have as many points as the longest vector in the set. In effect, we can visualize fluctuations in velocity from the start to the end of each session on the same scale. Data is represented as mean \pm standard error. (A-D) Orange represents data from PAE rats and black represents data from control animals.

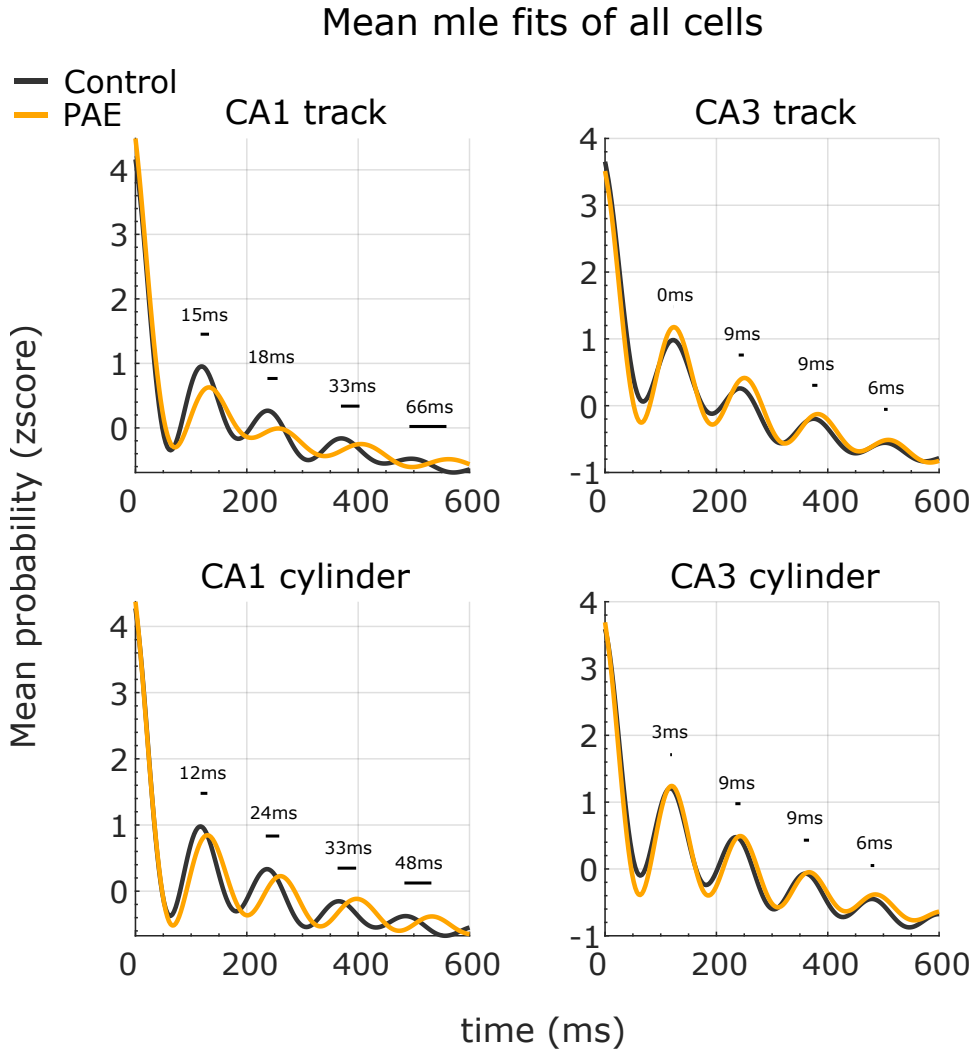


Figure S3: Mean maximum likelihood estimation fits for all cells. Related to Figure 5. While Figure 5C shows mean autocorrelogram fits of just spatially modulated cells, here we show mean fits from all theta rhythmic cells. Note that theta frequency is slightly slower in PAE cells. Dashes and numbers above each peak represent the time (ms) difference between the two groups at each theta peak.

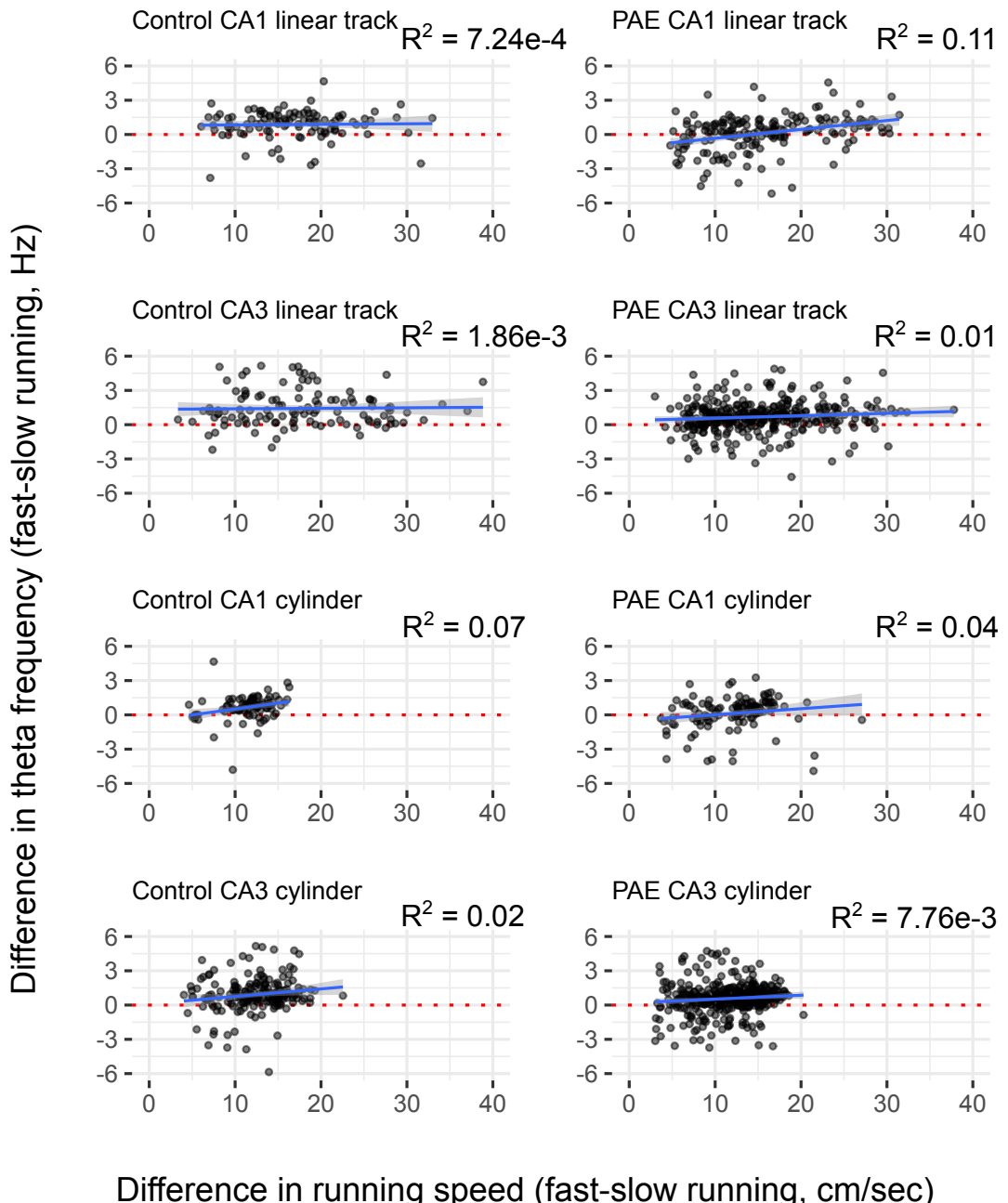


Figure S4: Association between intrinsic theta frequency and running speed. Related to Figure 6. Scatter plots show the relationship between the change in theta frequency (Hz) as a function of the magnitude difference between mean fast and slow running speed (cm/s). R-squared (R^2) for individual regression analyses are included in each subplot. Note that the change in running speed is a poor predictor of the change in frequency across all groups/conditions (R-squared values are ≤ 0.11). Values that fall along the red dashed line indicate no change in theta frequency. Line of best fit and corresponding confidence bounds for each regression are plotted in blue.

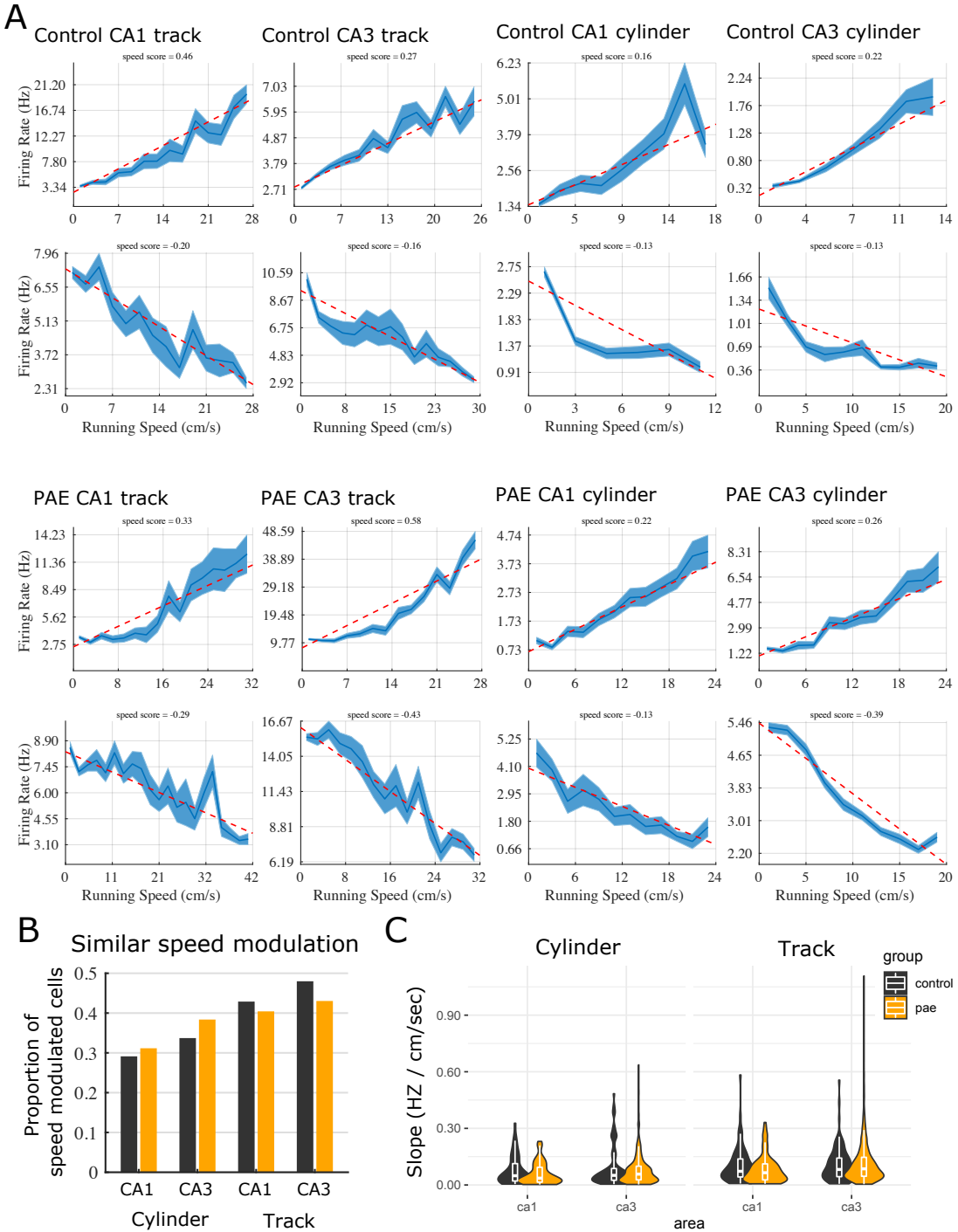


Figure S5: Speed modulation of HPC place cells are similar between groups. Related to Figure 6. (A) shows individual examples of positive and negative speed-modulated cells from both groups, HPC subregions, and spatial environments. The dashed red line indicates the linear function fit through the data. The solid blue line indicates the mean response, with blue shading denoting \pm standard error of the mean. Each cell's "speed score" or speed firing rate correlation (r) is indicated above each plot. (B) The proportion of cells that are speed modulated is similar between groups ($ps \geq 0.18$, WRS). (C) Slopes (Hz/cm/sec) are similar between groups ($ps \geq 0.098$, WRS). Slopes here are represented in absolute value.

	Saccharin Control (n = 9)	5% Ethanol Group (n = 8)
Daily four-hour 5% ethanol consumption	NA	1.96 ± 0.14 g/kg/d
Maternal weight gain during pregnancy	105 ± 7 g	120 ± 7 g
Litter size	10 ± 0.8 live births	11.9 ± 0.8 live births
Pup birth weight	7.79 ± 0.38 g	7.84 ± 0.56 g

Table S1: Impact of 5% ethanol consumption on maternal weight gain, litter size, and pup birth weight. Related to STAR Methods. All values are represented as mean \pm standard error of the mean.

Dependent Variable	n	Parameter estimate	Test	Test statistic	P-value	Effect measure	Effect size
Number of laps	C: 64, P: 111	C: 41, P: 40	Wilcoxon rank sum test	4182	0.05036	r	0.147
Linear track velocity	C: 64, P: 111	C: 9.35, P: 9.64	Wilcoxon rank sum test	3292	0.4214	r	0.060
Cylinder velocity	C: 57, P: 100	C: 8.35, P: 8.16	Wilcoxon rank sum test	3041	0.4868	r	0.055
Spatial Information Content linear track CA1	C: 220, P: 421	C: 0.51, P: 0.51	Wilcoxon rank sum test	48178	0.4015	r	0.033
Spatial Information Content linear track CA3	C: 215, P: 1049	C: 0.64, P: 0.40	Wilcoxon rank sum test	147395	1.234e-12	r	0.199
Spatial Information Content cylinder CA1	C: 162, P: 306	C: 0.72, P: 0.72	Wilcoxon rank sum test	24899	0.9356	r	0.003
Spatial Information Content cylinder CA3	C: 247, P: 839	C: 1.29, P: 0.61	Wilcoxon rank sum test	145298	<2.2e-16	r	0.291
Sparcity linear track CA1	C: 220, P: 421	C: 0.54, P: 0.55	Wilcoxon rank sum test	45640	0.7636	r	0.011
Sparcity linear track CA3	C: 215, P: 1049	C: 0.47, P: 0.60	Wilcoxon rank sum test	79562	9.765e-12	r	0.191
Sparcity cylinder CA1	C: 162, P: 306	C: 0.31, P: 0.33	Wilcoxon rank sum test	24907	0.931	r	0.004
Sparcity cylinder CA3	C: 247, P: 839	C: 0.20, P: 0.35	Wilcoxon rank sum test	64267	<2.2e-16	r	0.275
Peak firing rate linear track CA1	C: 220, P: 421	C: 7.62, P: 6.19	Wilcoxon rank sum test	51947	0.01134	r	0.100
Peak firing rate linear track CA3	C: 215, P: 1049	C: 11.38, P: 8.17	Wilcoxon rank sum test	137478	4.026e-07	r	0.142
Peak firing rate cylinder CA1	C: 162, P: 306	C: 6.83, P: 5.48	Wilcoxon rank sum test	28043	0.01931	r	0.108
Peak firing rate cylinder CA3	C: 247, P: 839	C: 9.44, P: 7.39	Wilcoxon rank sum test	120978	6.149e-05	r	0.121
Coherence linear track CA1	C: 220, P: 421	C: 2.51, P: 2.42	Wilcoxon rank sum test	50907	0.03893	r	0.081
Coherence linear track CA3	C: 215, P: 1049	C: 2.70, P: 2.42	Wilcoxon rank sum test	145828	1.2e-11	r	0.190
Coherence cylinder CA1	C: 162, P: 306	C: 2.19, P: 2.02	Wilcoxon rank sum test	29192	0.001551	r	0.146
Coherence cylinder CA3	C: 247, P: 839	C: 2.24, P: 2.07	Wilcoxon rank sum test	126441	1.38e-07	r	0.159
Stability linear track CA1	C: 220, P: 421	C: 0.79, P: 0.69	Wilcoxon rank sum test	56229	8.362e-06	r	0.175
Stability linear track CA3	C: 215, P: 1049	C: 0.83, P: 0.77	Wilcoxon rank sum test	132852	3.806e-05	r	0.115
Stability cylinder CA1	C: 162, P: 306	C: 0.43, P: 0.24	Wilcoxon rank sum test	30629	2.699e-05	r	0.194
Stability cylinder CA3	C: 247, P: 839	C: 0.52, P: 0.36	Wilcoxon rank sum test	129414	2.615e-09	r	0.180
Spatial correlation linear track CA1	C: 220, P: 421	C: 0.16, P: 0.35	Wilcoxon rank sum test	20555	0.0001676	r	0.171
Spatial correlation linear track CA3	C: 215, P: 1049	C: 0.21, P: 0.19	Wilcoxon rank sum test	67057	0.8464	r	0.006
Directionality index linear track CA1	C: 220, P: 421	C: 0.30, P: 0.24	Wilcoxon rank sum test	28819	0.06507	r	0.084
Directionality index linear track CA3	C: 215, P: 1049	C: 0.32, P: 0.19	Wilcoxon rank sum test	81396	1.495e-05	r	0.138
Mean angle of Rotation cylinder CA1	C: 96, P: 148	C: 44.80, P: 82.84	Watson Williams	6.466	0.0117	na	na
Mean angle of rotation cylinder CA3	C: 108, P: 398	C: 246.40, P: 73.20	Watson Williams	82.087	<2.2e-16	na	na
Distribution of angles CA3 control	108	na	Rayleigh test of nonuniformity	24.380	9.4667e-12	na	na
Distribution of angles CA1 PAE	148	na	Rayleigh test of nonuniformity	3.012	0.0488	na	na
Distribution of angles CA3 PAE	398	na	Rayleigh test of nonuniformity	31.677	9.4583e-15	na	na
Distribution of angles around 90 CA1 control	96	na	V test of nonuniformity	11.719	0.0230	na	na
Distribution of angles around 90 CA3 control	108	na	V test of nonuniformity	59.602	2.1244e-12	na	na
Distribution of angles around 90 CA1 PAE	148	na	V test of nonuniformity	-16.531	0.9878	na	na
Distribution of angles around 90 CA3 PAE	398	na	V test of nonuniformity	107.529	1.2434e-14	na	na
Normalized delta firing rate CA1	C: 96, P: 148	C: 0.27, P: 0.18	Wilcoxon rank sum test	29859	1.939e-05	r	0.199
Normalized delta firing rate CA3	C: 108, P: 398	C: 0.43, P: 0.18	Wilcoxon rank sum test	142264	<2.2e-16	r	0.275
Delta spatial information content CA1	C: 96, P: 148	C: 0.08, P: 0.04	Wilcoxon rank sum test	7512	0.2792	r	0.068
Delta spatial information content CA3	C: 108, P: 398	C: -0.07, P: 0.02	Wilcoxon rank sum test	26962	0.003245	r	0.120
Delta sparsity CA1	C: 96, P: 148	C: -0.02, P: -0.00	Wilcoxon rank sum test	6532	0.4595	r	0.046
Delta sparsity CA3	C: 108, P: 398	C: 0.02, P: -0.00	Wilcoxon rank sum test	36150	0.02879	r	0.089
Proportion of sig. theta cylinder ca1	C: 162, P: 306	C: 0.89, P: 0.74	Chi-squared	13.928	1.8988e-04	V	0.020
Proportion of sig. theta cylinder ca3	C: 247, P: 839	C: 0.95, P: 0.84	Chi-squared	32.012	1.5319e-08	V	0.018
Proportion of sig. theta linear track ca1	C: 220, P: 421	C: 0.84, P: 0.85	Chi-squared	0.8192	0.3654	V	0.001
Proportion of sig. theta linear track ca3	C: 215, P: 1049	C: 0.94, P: 0.85	Chi-squared	15.554	8.0171e-05	V	0.009
Theta frequency cylinder ca1	C: 162, P: 306	C: 8.42, P: 7.81	Wilcoxon rank sum test	14755	7.215e-10	r	0.360
Theta frequency cylinder ca3	C: 247, P: 839	C: 8.47, P: 8.12	Wilcoxon rank sum test	75874	4.921e-10	r	0.226
Theta frequency linear track ca1	C: 220, P: 421	C: 8.44, P: 7.65	Wilcoxon rank sum test	21929	5.534e-13	r	0.378
Theta frequency linear track ca3	C: 215, P: 1049	C: 8.41, P: 7.99	Wilcoxon rank sum test	51565	1.983e-05	r	0.158
Frequency difference cylinder ca1	C: 89, P: 117	C: 0.80, P: 0.51	Wilcoxon rank sum test	6382	0.005565	r	0.193
Frequency difference cylinder ca3	C: 179, P: 408	C: 0.78, P: 0.64	Wilcoxon rank sum test	42457	0.001688	r	0.129
Frequency difference linear track ca1	C: 106, P: 173	C: 1.02, P: 0.29	Wilcoxon rank sum test	12510	3.277e-07	r	0.305
Frequency difference linear track ca3	C: 115, P: 345	C: 1.19, P: 0.69	Wilcoxon rank sum test	24804	5.76e-05	r	0.187
Proportion speed modulated frequency cylinder ca1	C: 125, P: 170	C: 0.47, P: 0.34	Chi-squared	5.151	0.0232	V	0.012
Proportion speed modulated frequency cylinder ca3	C: 219, P: 552	C: 0.52, P: 0.43	Chi-squared	5.251	0.0219	V	0.004
Proportion speed modulated frequency track ca1	C: 129, P: 243	C: 0.52, P: 0.35	Chi-squared	10.422	0.0012	V	0.019
Proportion speed modulated frequency track ca3	C: 145, P: 580	C: 0.43, P: 0.40	Chi-squared	0.462	0.4967	V	4.52e-04
Proportion of sig. phase precession cylinder ca1	C: 162, P: 306	C: 0.25, P: 0.17	Chi-squared	2.489	0.1146	V	0.072
Proportion of sig. phase precession cylinder ca3	C: 247, P: 839	C: 0.37, P: 0.27	Chi-squared	14.183	0.0001658	V	0.096
Proportion of sig. phase precession linear track ca1	C: 220, P: 421	C: 0.28, P: 0.21	Chi-squared	2.49	0.1146	V	0.06
Proportion of sig. phase precession linear track ca3	C: 215, P: 1049	C: 0.49, P: 0.37	Chi-squared	4.706	0.03005	V	0.06
Circular-linear correlation cylinder ca1	C: 162, P: 306	C: -0.01, P: -0.01	Wilcoxon rank sum test	25599	0.5594	r	0.026
Circular-linear correlation cylinder ca3	C: 247, P: 839	C: -0.04, P: -0.02	Wilcoxon rank sum test	95289	0.05462	r	0.058
Circular-linear correlation linear track ca1	C: 220, P: 421	C: 0.01, P: 0.01	Wilcoxon rank sum test	46199	0.9604	r	0.001
Circular-linear correlation linear track ca3	C: 215, P: 1049	C: 0.01, P: 0.00	Wilcoxon rank sum test	116127	0.4909	r	0.019

Table S2: Table showing each statistical test conducted from the main texts. Related to STAR Methods. n = sample sizes, c = control, p = PAE